

Supplementary Information

Small-pore driven high capacitance in a hierarchical carbon from carbonization of Ni-MOF-74 at low temperatures

J. A. Carrasco,<sup>a</sup> J. Romero,<sup>a</sup> G. Abellán,<sup>b</sup> J. Hernández-Saz,<sup>c</sup> S. I. Molina,<sup>c</sup> C. Martí-Gastaldo<sup>\*a</sup> and E. Coronado<sup>a</sup>

[a] Instituto de Ciencia Molecular, Universitat de València, Catedrático José Beltrán 2, 46980, Paterna (Spain). E-mail: [carlos.marti@uv.es](mailto:carlos.marti@uv.es)

[b] Department of Chemistry and Pharmacy, University Erlangen-Nürnberg, Henkestr. 42, 91054 Erlangen (Germany).

[c] Departamento de Ciencia de los Materiales e I.M. y Q.I., Facultad de Ciencias, IMEYMAT, Universidad de Cádiz, Campus Río San Pedro, s/n, 11510, Cádiz (Spain).

Table of contents:

<b>SI 1.</b> General considerations: starting materials and physical characterization.....	3
<b>SI 2.</b> Synthesis of materials and experimental details. ....	4
<b>SI 3.</b> PXRD of as-made, activated and Ni-MOF-74/FA.....	5
<b>SI 4.</b> Scanning Electron Microscopy (SEM) images of Ni-MOF-74/FA. ....	7
<b>SI 5.</b> N <sub>2</sub> adsorption/desorption isotherms at 77K of activated and Ni-MOF-74/FA. ....	8
<b>SI 6.</b> Thermogravimetric analysis of activated Ni-MOF-74 and Ni-MOF-74/FA ....	9
<b>SI 7.</b> PXRD of Ni-MOF-74/C <sub>250</sub> , Ni/C <sub>450</sub> , Ni/C <sub>800</sub> and Ni/C <sub>1000</sub> . ....	10
<b>SI 8.</b> N <sub>2</sub> adsorption/desorption isotherms at 77K of Ni-MOF-74/C <sub>250</sub> . ....	12
<b>SI 9.</b> Scanning Electron Microscopy (SEM) images of Ni-MOF-74/C <sub>250</sub> , Ni/C <sub>450</sub> , Ni/C <sub>800</sub> and Ni/C <sub>1000</sub> . ....	13
<b>SI 10.</b> Imaging of the internal cross section of Ni/C <sub>450</sub> , Ni/C <sub>800</sub> and Ni/C <sub>1000</sub> by ion-induced secondary electron microscopy by using Focused Ion Beam-Scanning Electron Microscopy (FIB-SEM). ....	14
<b>SI 11.</b> TEM images of Ni/C <sub>450</sub> , Ni/C <sub>800</sub> and Ni/C <sub>1000</sub> and size distribution of nanoparticles ....	15
<b>SI 12.</b> Field dependence of the magnetization at 300 K of Ni/C <sub>1000</sub> .....	18
<b>SI 13.</b> Raman spectra of Ni/C <sub>450</sub> , Ni/C <sub>800</sub> and Ni/C <sub>1000</sub> collected on bulk pellets at room temperature. ....	19
<b>SI 14.</b> Analysis of N <sub>2</sub> adsorption/desorption isotherms at 77K of Ni/C <sub>450</sub> , Ni/C <sub>800</sub> and Ni/C <sub>1000</sub> . ....	20
<b>SI 15.</b> Electron Probe Microanalysis of C <sub>450</sub> , C <sub>800</sub> and C <sub>1000</sub> .....	21
<b>SI 16.</b> CO <sub>2</sub> adsorption isotherms at 273K of C <sub>450</sub> , C <sub>800</sub> and C <sub>1000</sub> . ....	22
<b>SI 17.</b> Analysis of N <sub>2</sub> and CO <sub>2</sub> adsorption/desorption isotherms at 77 and 273K of C <sub>450</sub> , C <sub>800</sub> and C <sub>1000</sub> . ....	23
<b>SI 18.</b> Electrochemistry of C <sub>450</sub> , C <sub>800</sub> and C <sub>1000</sub> . ....	24
<b>SI 19.</b> XPS spectra of C <sub>450</sub> . ....	25
<b>SI 20.</b> Specific capacitances, textural properties and calcination temperatures of a representative set of MOF-derived carbons measured in a three-electrode system. ....	27
<b>SI 21.</b> Long-term stability cycling of C <sub>450</sub> studied at 10 A.g <sup>-1</sup> upon 10.000 charge-discharge cycles. ....	28
<b>SI 22.</b> High-Resolution Transmission Electron Microscopy study of carbons. ....	28
<b>SI 23.</b> References. ....	31

## SI 1. General considerations: starting materials and physical characterization.

### Materials and reagents.

Ni(NO<sub>3</sub>)·6H<sub>2</sub>O (99.99%), dihydroxyterephthalic acid (98%) and furfuryl alcohol (98) were purchased from Sigma-Aldrich, and used as received. N,N-Dimethylformamide (≥ 99.8%) and absolute ethanol (≥ 99.9%) were purchased from Scharlau. Ultrapure water from Milli-Q equipment was used when required. All reagents and solvents were used without any previous purification unless specified.

### Physical characterization.

Carbon, nitrogen and hydrogen contents were determined by microanalytical procedures using a LECO CHNS. Infrared spectra were recorded in an Agilent Cary 630 FTIR Spectrometer directly with no need of KBr pellets. Thermogravimetric analysis were carried out with a Mettler Toledo TGA/SDTA 851 apparatus between 25 and 800 °C under ambient conditions.

XRD patterns were collected in a PANalytical X'Pert PRO diffractometer using copper radiation (Cu K $\alpha$  = 1.5418 Å) with an X'Celerator detector, operating at 40 mA and 45 kV. Profiles were collected in the 2° < 2 $\theta$  < 60° range with a step size of 0.017°.

Particle morphologies and dimensions were studied with a Hitachi S-4800 scanning electron microscope at an accelerating voltage of 20 keV, over metalized samples with a mixture of gold and palladium during 30 s. HR-TEM studies were carried out on a Tecnai G2 F20 microscope operating at 200 kV. Samples were prepared by dropping a suspension of the sample in ethanol on a lacey formvar/carbon copper grid (300 mesh). FEI dual-beam FIB-SEM Quanta 200 3D equipment with the Ga column operating at 30 kV was used to mill and acquire the ion-induced secondary electron images of the cross-sections of the Ni/C composites.

Surface area, pore size and volume values were calculated from nitrogen adsorption-desorption isotherms (-196°C) recorded on a AUTOSORB-6 apparatus. Samples were degassed for 4 hours at 150°C and 10<sup>-6</sup> Torr prior to analysis. Surface areas were estimated according to the BET model, and pore size dimensions were calculated by the solid density functional theory (QSDFT) for the adsorption branch assuming a cylindrical pore model.

Magnetic measurements were carried out with a Quantum Design superconducting quantum interference device (SQUID) MPMS-XL-5. The susceptibility data were corrected from the diamagnetic contributions of the atomic constituents of the samples as deduced from Pascal's constant tables and the sample holder. Magnetization studies were performed between -5 and +5 T at a constant temperature of 300 K.

Raman measurements were carried out in a Jobin-Yvon LabRam HR 800 Raman Microscope at room temperature with the 532 nm line of an Ar ion laser as an excitation source. X-ray Photoelectron Spectroscopy (XPS) was performed ex situ at the X-ray Spectroscopy Service at the Universidad de Alicante using a K-Alpha X-ray photoelectron spectrometer system (Thermo Scientific). All spectra were collected using Al K $\alpha$  radiation (1486.6 eV), monochromatized by a twin crystal monochromator, yielding a focused X-ray spot (elliptical in shape with a major axis length of 400  $\mu$ m) at 3 mA·C and 12 kV. The alpha hemispherical analyzer was operated in the constant energy mode with survey scan pass energies of 200 eV to measure the whole energy band and 50 eV in a narrow scan to selectively measure the particular elements. XPS data were analyzed with Avantage software. A smart background function was used to approximate the experimental backgrounds. Charge compensation was achieved with the system flood gun that provides low energy electrons and low energy argon ions from a single source.

Electrochemical Measurements. The materials were mixed with acetylene black and PVDF in a mass ratio of 80:10:10 in ethanol and deposited in a nickel foam electrode. The as-prepared nickel foam electrodes were dried overnight at 80 °C and pressed. Each working electrode contained about 1 mg of electroactive material and had a geometric surface area of about 1 cm<sup>2</sup>. A typical three-electrode experimental cell equipped with a stainless steel plate having 4 cm<sup>2</sup> of surface area as the counter electrode and a Metrohm Ag/AgCl (3 M KCl) as the reference electrode was used for the electrochemical characterization of the nanocomposite materials trapped by the working electrodes. All the electrochemical measurements were carried out in 6 M KOH aqueous solutions as the electrolyte. Ultrapure water was obtained from Milli-Q equipment. All the electrochemical experiments were performed at room temperature using an AUTOLAB PGSTAT 100 potentiostat-galvanostat controlled by GEPES electrochemical software. The specific capacitance (C) was calculated from the cyclic chronopotentiometric curves according to Equation 1:

$$C = I/m \int V(t)dt \quad (1)$$

where  $I$  is the charge/discharge current and  $m$  the weight in grams of the active material in the electrode layer.

## SI 2. Synthesis of materials and experimental details.

**Ni-MOF-74** was synthesized as described according to reported methodology.<sup>1</sup> In a typical procedure, 4.756 g of Ni(NO<sub>3</sub>)-6H<sub>2</sub>O and 0.956 g of dihydroxyterephthalic acid were dissolved in 400 mL of a mixture of DMF : EtOH : Milli-Q H<sub>2</sub>O (1 : 1 : 1). The solution was then sonicated in an ultrasound bath for 10 – 15 min and heated in an oven at 100 °C for 24 h. The mixture was cooled at room temperature, filtered and washed thoroughly with Milli-Q water and EtOH (53% yield calculated for Ni).

**Activation of Ni-MOF-74.** As-made Ni-MOF-74 was heated at 200 °C for 4 hours under reduced pressure (10<sup>-3</sup> mbar). The experimental weight loss of 25% calculated from thermogravimetric analysis is consistent with the removal of 1.6 water molecules occupying the pores. The solid was stored in static vacuum at room temperature.

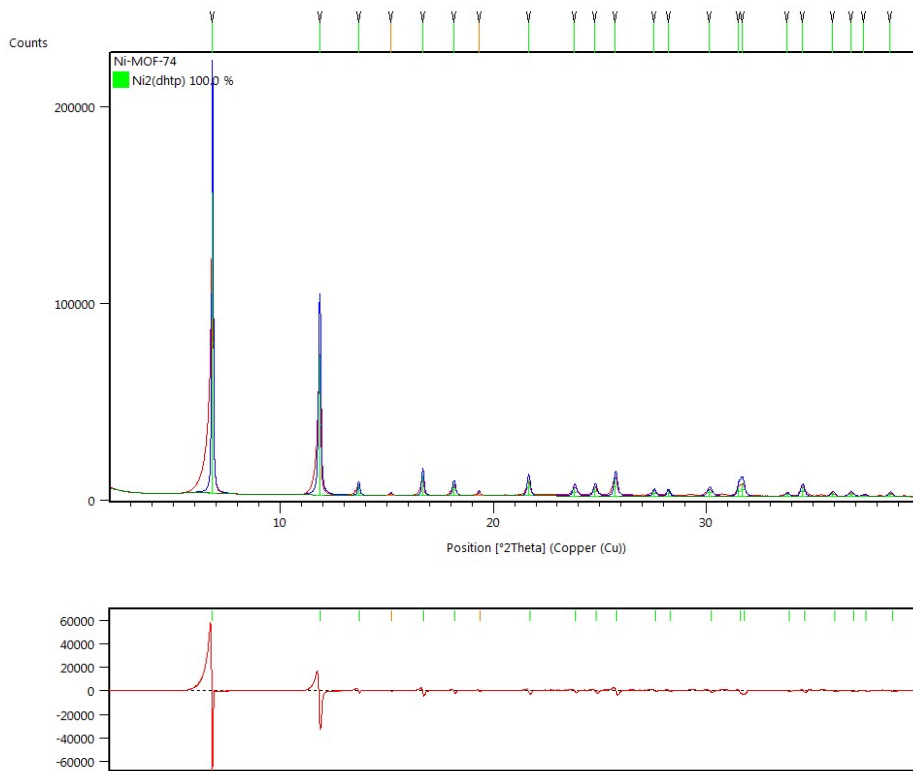
**Ni-MOF-74/FA.** For the loading with furfuryl alcohol (FA), 1 g of activated Ni-MOF-74 was dissolved in 20 mL of FA and heated at 60 °C for 12 h with continuous magnetic stirring. After that, the mixture was filtered and thoroughly washed with EtOH to remove non-infiltrated FA molecules that might remain stuck to the outer surface of the crystals. The solid gains a 30 % in weight after loading. This is consistent with the loading of approximately 0.4 molecules found for the TG analysis (Fig. SI6). The solid was stored in a glass vial at room temperature.

**Synthesis of Ni/C composites.** Ni-MOF-74/FA was transferred to a quartz vessel and charged into a tubular furnace. All samples were calcined under a flow of N<sub>2</sub> (100 mL.min<sup>-1</sup>) with heating/cooling rates of 5 °C.min<sup>-1</sup>. Solid was heated at 250 °C for 6 hours, for polymerization of the FA molecules in the pores, followed by carbonization at 450, 800 and 1000 °C for 8 hours to produce: Ni/C<sub>450</sub>, Ni/C<sub>800</sub> and Ni/C<sub>1000</sub>.

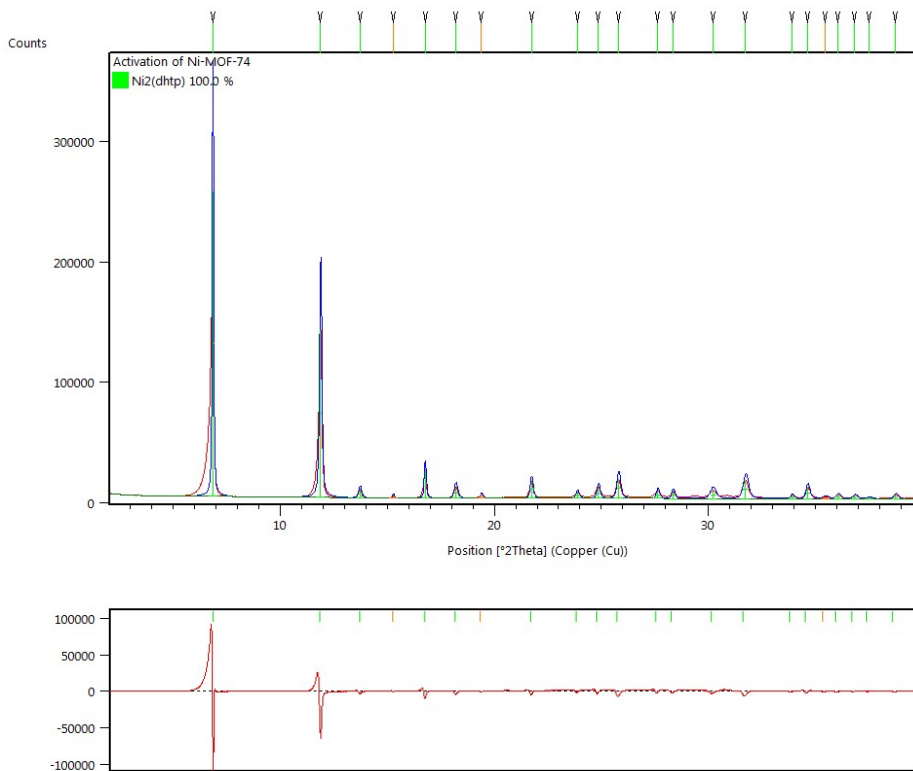
**Isolation of nanocarbons.** Ni/C<sub>450</sub> was soaked in 50 mL of HNO<sub>3</sub>(aq) 2.2M and heated for 2 hours at 80 °C in static conditions. This process was carried out for a complete metal leaching in order to produce C<sub>450</sub>. Complete removal of Ni from the samples was confirmed by Scanning Electron Microscopy coupled to Electron Probe Microanalysis (Fig. SI15).

SI 3. PXRD of as-made, activated Ni-MOF-74 and Ni-MOF-74/FA. Refinement against the unit cell calculated from the atomic positional parameters of the single-crystal data available CCDC 288477.<sup>2</sup> Difference plot is represented with a red line in the panel below. Refined cell parameters calculated with X'Pert HighScore Plus:

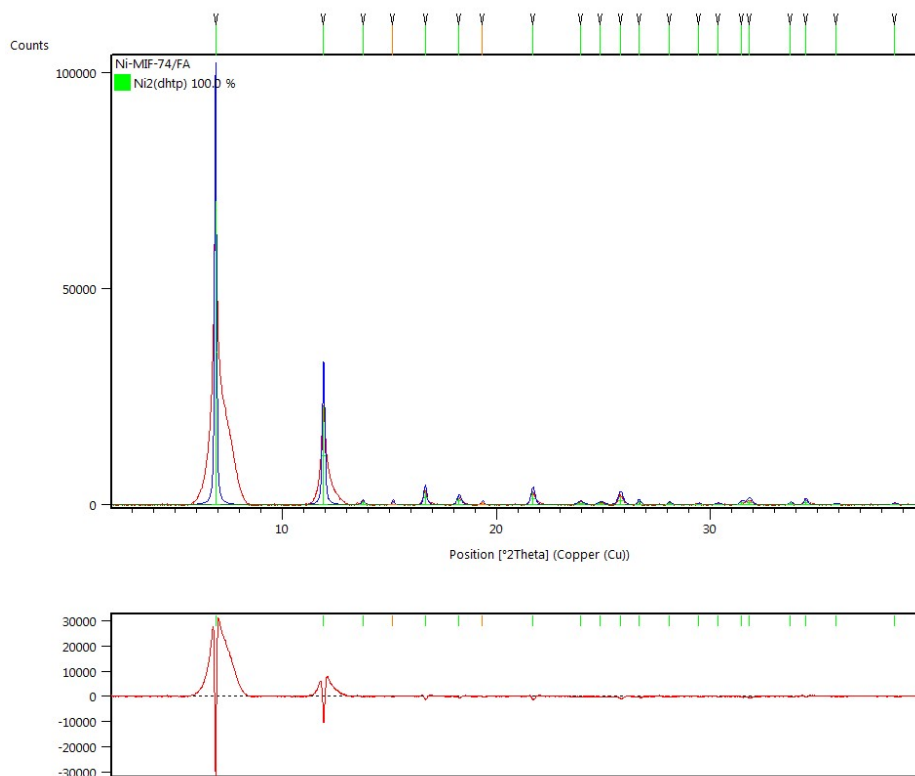
as-made Ni-MOF-74: Hexagonal, R-3;  $a = b = 25.87(5)$   $c = 6.79(4)$  Å;  $\alpha = \beta = 90^\circ$ ;  $\gamma = 120^\circ$ ;  $V = 3936.7$  Å<sup>3</sup>.



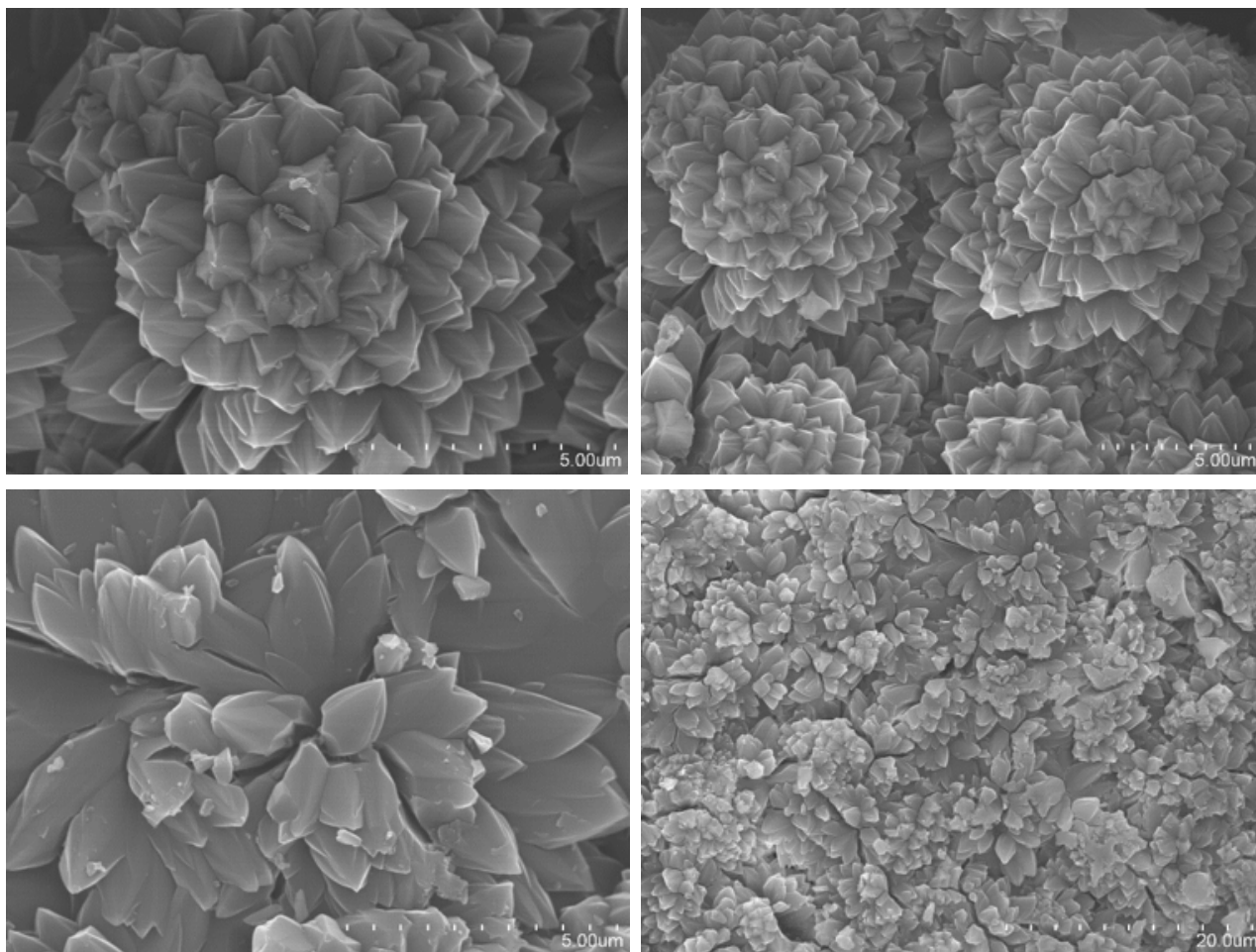
degassed Ni-MOF-74: Hexagonal, R-3;  $a = b = 25.77(6)$   $c = 6.77(4)$  Å;  $\alpha = \beta = 90^\circ$ ;  $\gamma = 120^\circ$ ;  $V = 3892.71$  Å<sup>3</sup>.



Ni-MOF-74/FA: Hexagonal, R-3;  $a = b = 25.86(6)$   $c = 6.96(5)$  Å;  $\alpha = \beta = 90^\circ$ ;  $\gamma = 120^\circ$ ;  $V = 4031.52$  Å<sup>3</sup>.

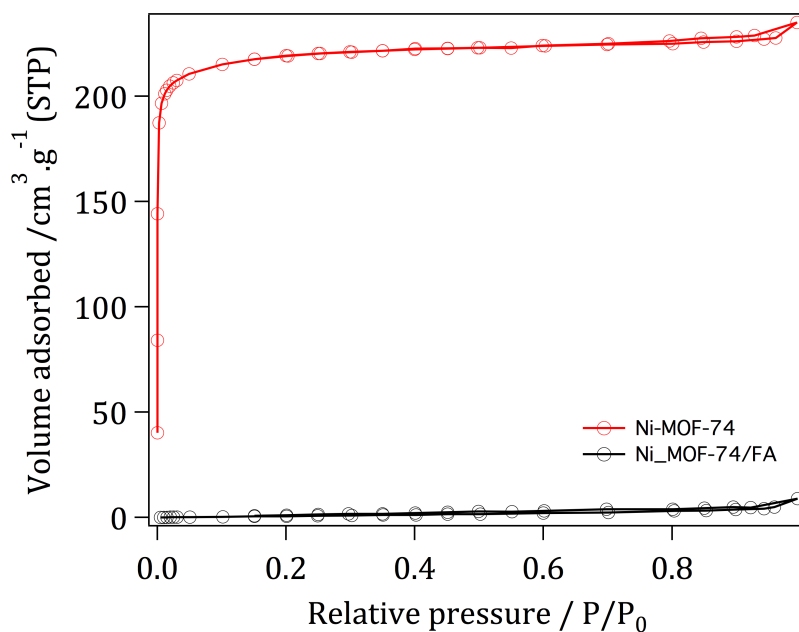


SI 4. Scanning Electron Microscopy (SEM) images of Ni-MOF-74/FA.



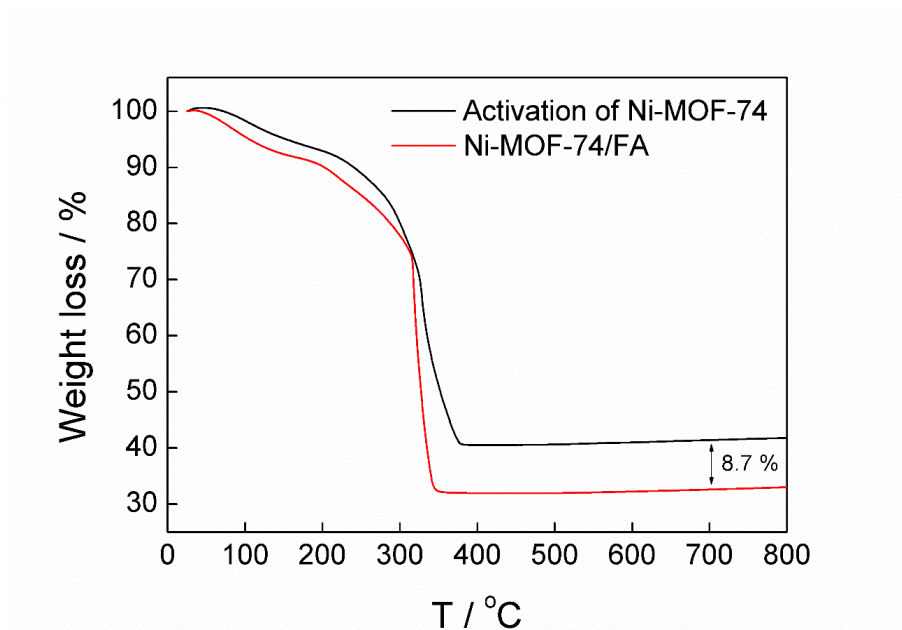
After solvent removal and FA loading, Ni-MOF-74/FA retains the crystal size and rose-type morphology of the as-made solid. Equivalent characteristics have been reported for isostructural Mg-MOF-74 prepared by solvothermal reaction.<sup>3</sup>

SI 5. N<sub>2</sub> adsorption/desorption isotherms at 77K of activated Ni-MOF-74 (red) and Ni-MOF-74/FA (black).



Nitrogen adsorption/desorption experiments were used to confirm the expected porosity of Ni-MOF-74 and confirm the loading of the pores with furfuryl alcohol. Ni-MOF-74 displays reversible uptake of N<sub>2</sub> with a type-I isotherm. The BET surface area of 883.1 m<sup>2</sup>.g<sup>-1</sup>, calculated from the linear region at low-P, is slightly below the value reported in the literature likely due to differences in the activation protocol.<sup>2</sup> The amount of physisorbed N<sub>2</sub> decreases drastically for Ni-MOF-74/FA with a BET of 4.1 m<sup>2</sup>.g<sup>-1</sup>. This is consistent with a complete filling of the pores.

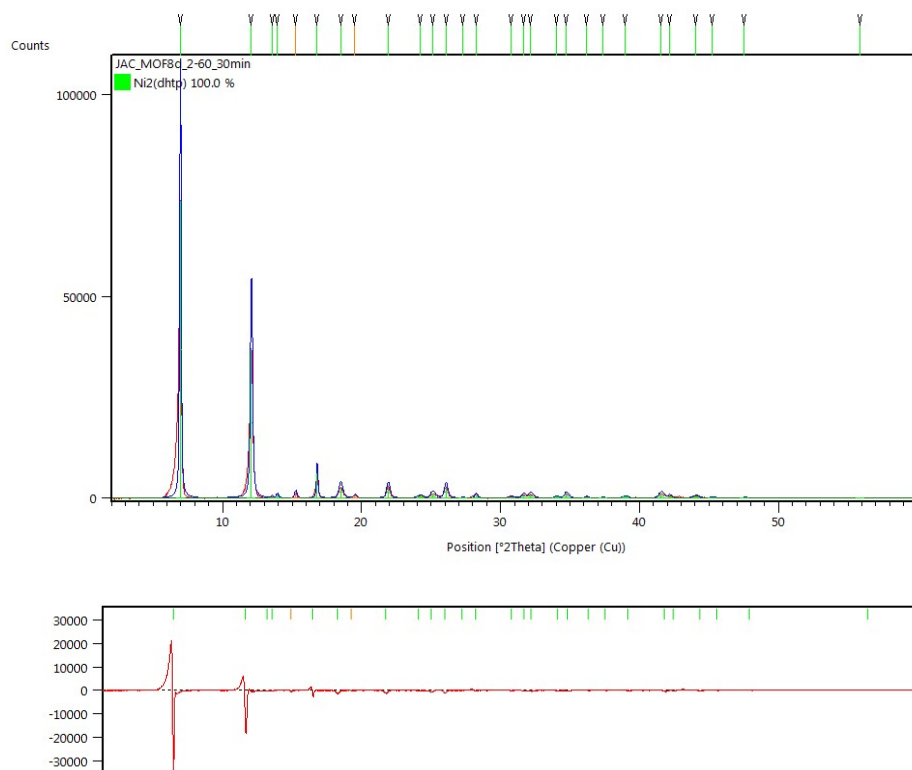
SI 6. Thermogravimetric analysis (TGA) of Ni-MOF-74 after activation (black) and Ni-MOF-74 loaded with furfuryl alcohol (red).



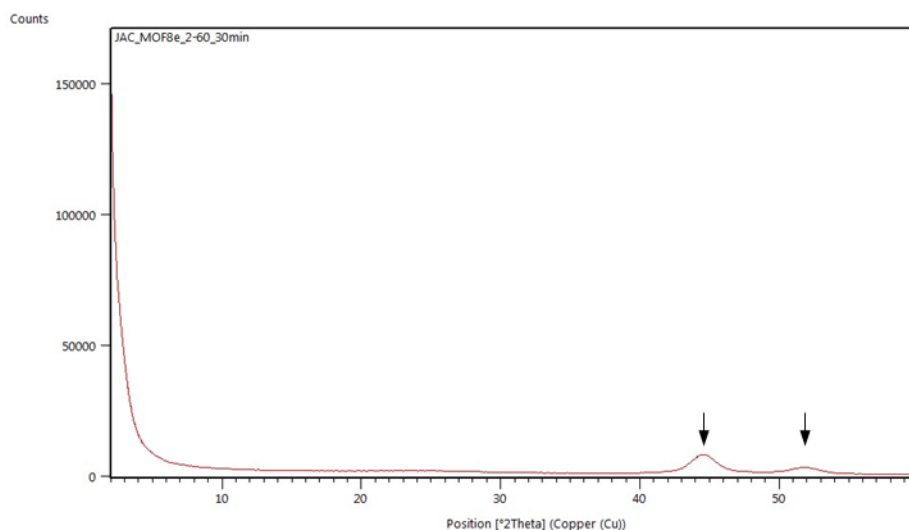
The weight loss difference of 8.7 %, between FA loaded and activated Ni-MOF-74, can be linked to the presence of 0.4 molecules of furfuryl alcohol per unit of  $[\text{Ni}_2(\text{dhtp})]$ . This agrees well with the 0.55 molecules estimated from CHN analysis.

SI 7. PXRD of Ni-MOF-74/C<sub>250</sub>, Ni/C<sub>450</sub>, Ni/C<sub>800</sub> and Ni/C<sub>1000</sub>. Refinement against the unit cell calculated from the atomic positional parameters of the single-crystal data available CCDC 288477.<sup>2</sup> Difference plot is represented with a red line in the panel below. Refined cell parameters calculated with X'Pert HighScore Plus:

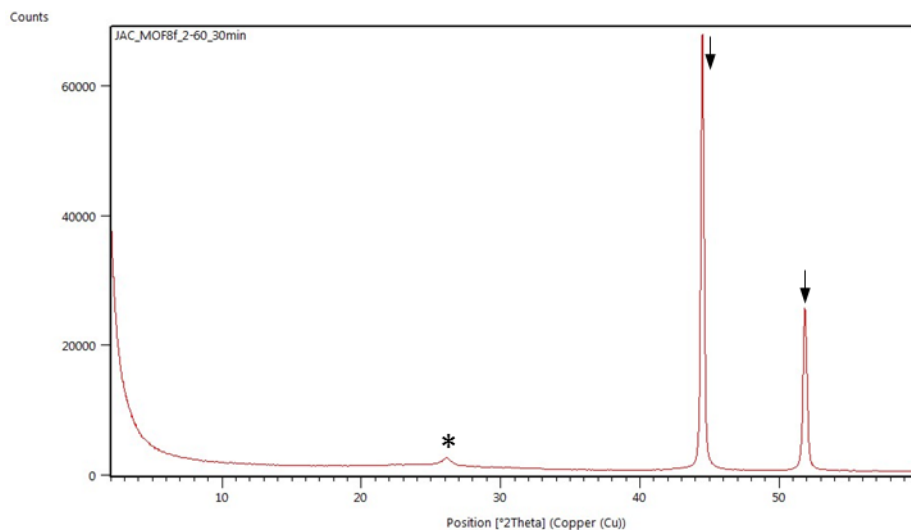
Ni-MOF-74/C<sub>250</sub>: Hexagonal, R-3;  $a = b = 25.70(4)$   $c = 6.81(1)$  Å;  $\alpha = \beta = 90^\circ$ ;  $\gamma = 120^\circ$ ;  $V = 3891.5$  Å<sup>3</sup>.



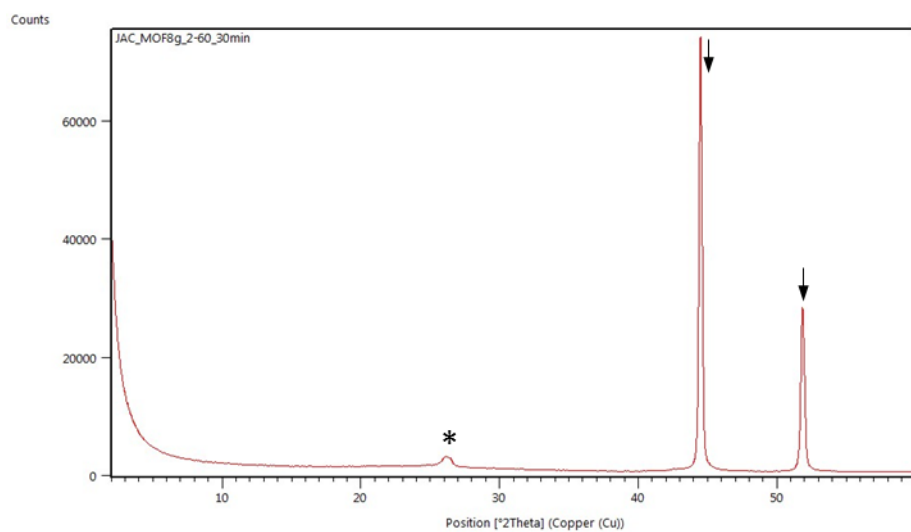
Ni/C<sub>450</sub>: Original PXRD fingerprint of Ni-MOF74 disappears to give rise to two broad shoulders at 44.5 and 51.8°. This agrees well with the collapse of the structure of the MOF linked to its decomposition and the incipient formation of Ni. The peaks marked by arrows can be indexed to Ni (ICDD-JCPDS Card No. 04-0850).



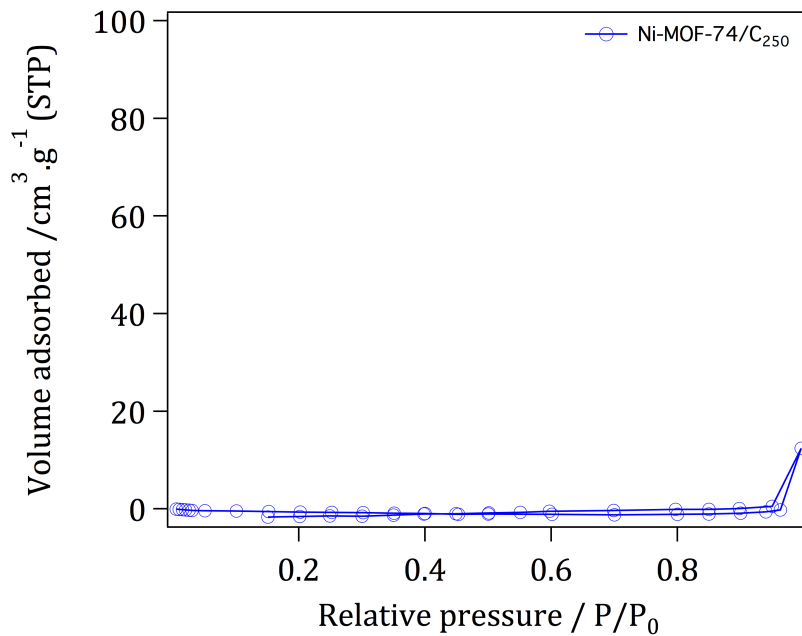
Ni/C<sub>800</sub>: PXRD dominated by sharp, intense diffraction lines associated to metallic Ni (marked by arrows) along with a broad shoulder centered at 26.2° (3.39 Å; marked by asterisk), that agrees well with the position of (001) in graphite ( $d_{001}= 3.36 \text{ \AA}$ ). Besides higher temperature, this suggests that the formation of crystalline Ni clusters favours the formation of more crystalline carbon in line with its catalytic activity for carbon decomposition.



Ni/C<sub>1000</sub>: Almost identical to Ni/C<sub>800</sub>. Consistent with the presence of metallic Ni (marked by arrows) and crystalline graphitic carbon (marked by asterisk).



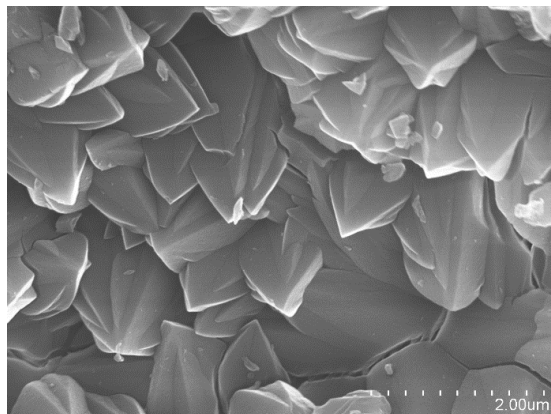
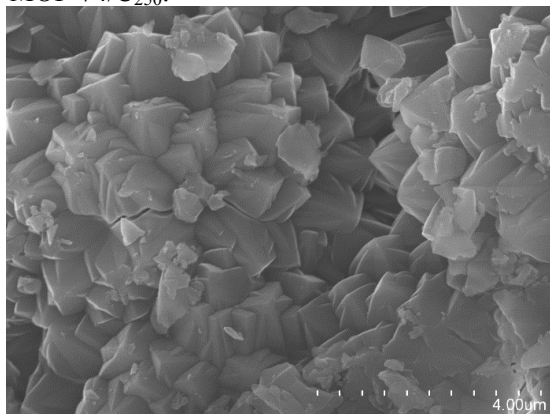
SI 8. N<sub>2</sub> adsorption/desorption isotherms at 77K of Ni-MOF-74/C<sub>250</sub>.



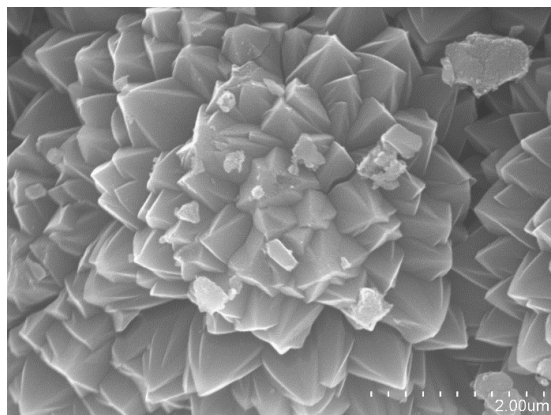
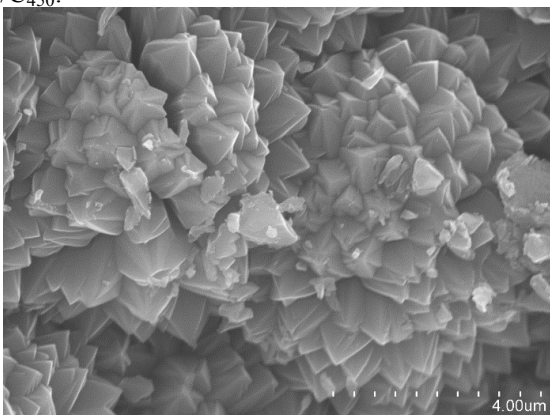
The amount of physisorbed N<sub>2</sub> is negligible, which agrees well with the blocking of the pores by the amorphous carbon formed as result of the polymerization of FA molecules.

SI 9. Scanning Electron Microscopy (SEM) images of Ni-MOF-74/C<sub>250</sub>, Ni/C<sub>450</sub>, Ni/C<sub>800</sub> and Ni/C<sub>1000</sub>.

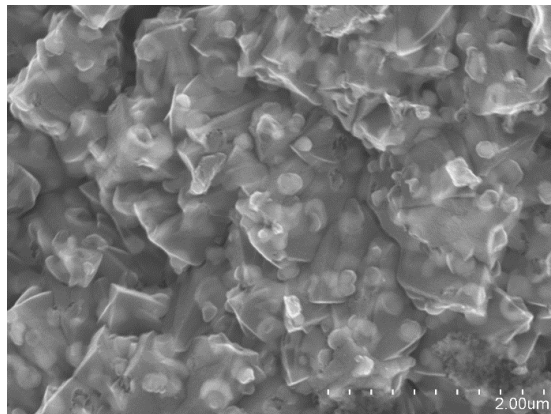
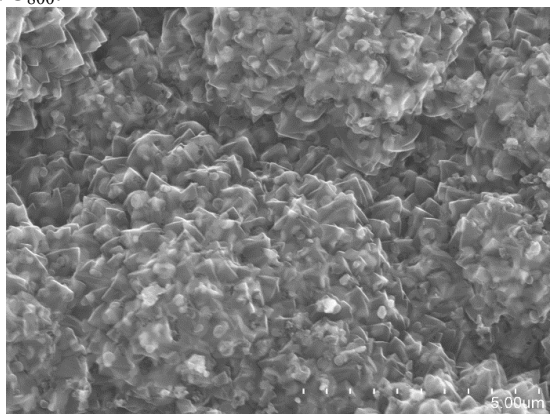
Ni-MOF-74/C<sub>250</sub>:



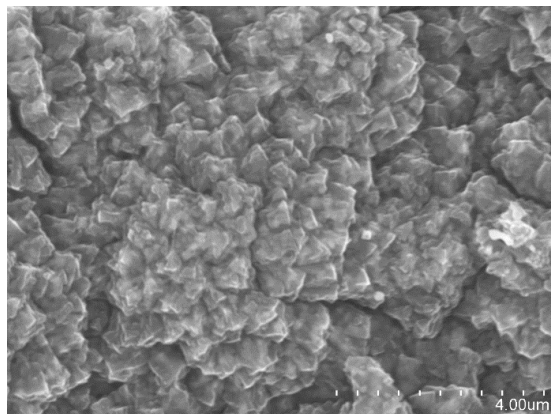
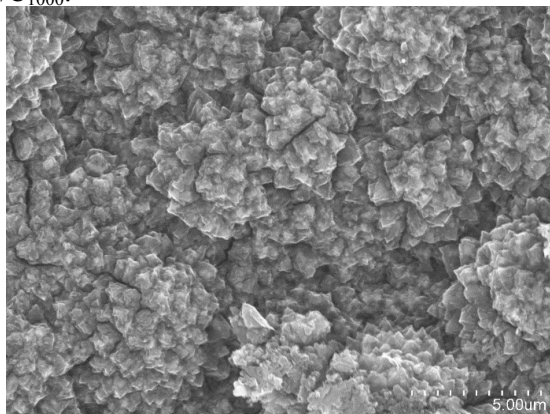
Ni/C<sub>450</sub>:



Ni/C<sub>800</sub>:

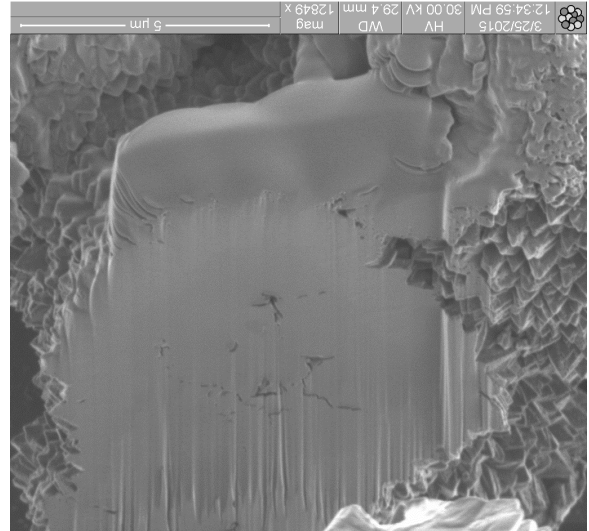
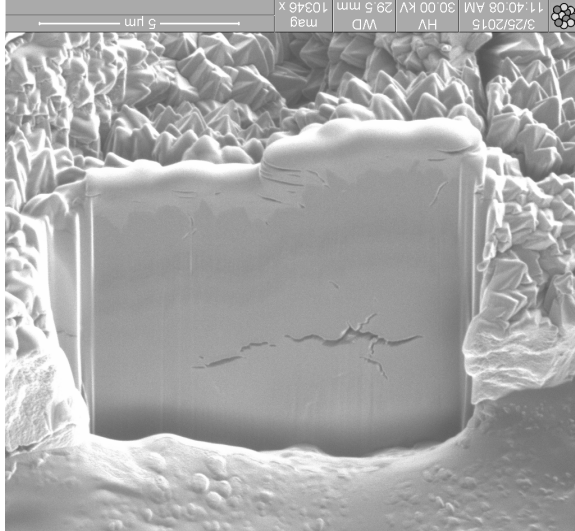


Ni/C<sub>1000</sub>:

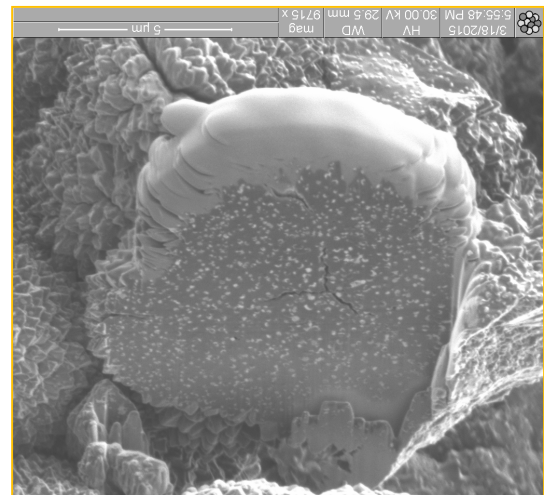
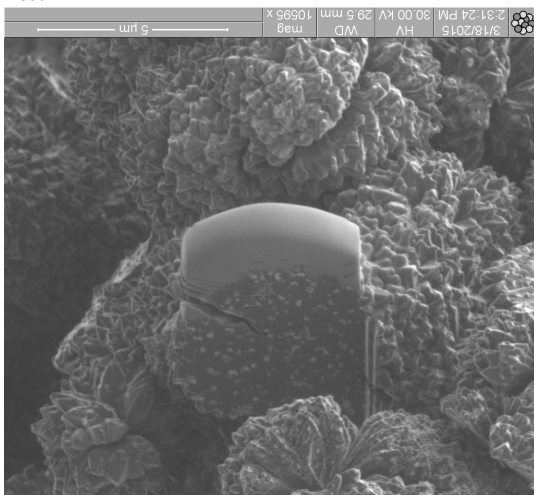


SI 10. Imaging of the internal cross section of Ni/C<sub>450</sub>, Ni/C<sub>800</sub> and Ni/C<sub>1000</sub> by ion-induced secondary electron microscopy by using Focused Ion Beam-Scanning Electron Microscopy (FIB-SEM). These images correspond to different FIB sections complementary to those included in the main text. A trench was carved through a selected area of the crystal followed by polishing of the cross-section prior to taking an ion-induced secondary electron image.

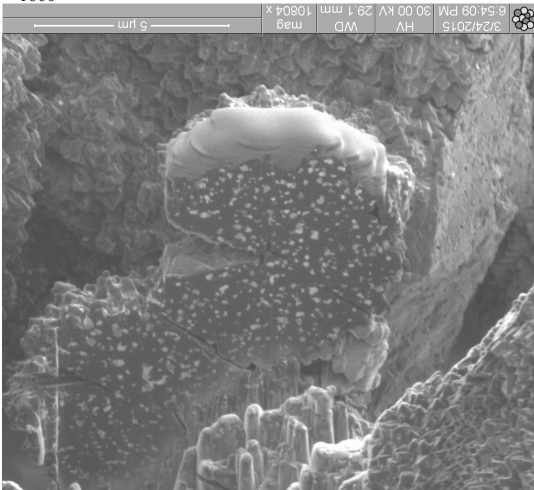
Ni/C<sub>450</sub>:



Ni/C<sub>800</sub>:

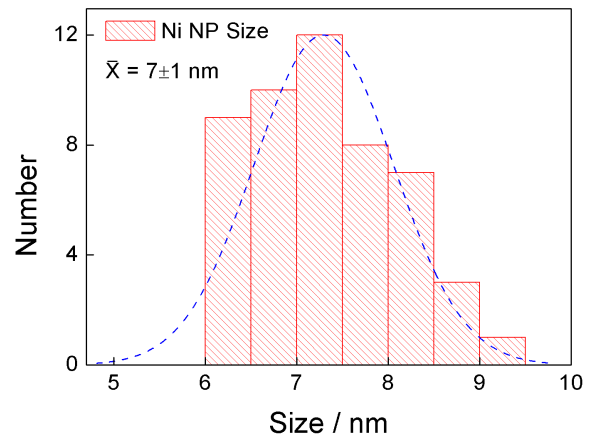
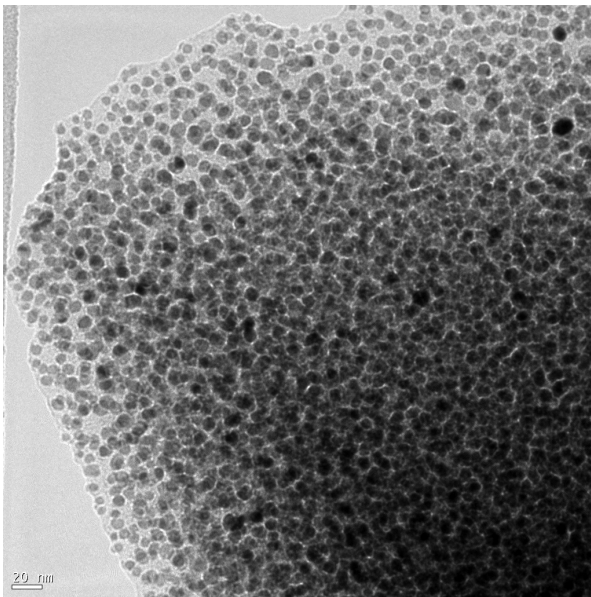
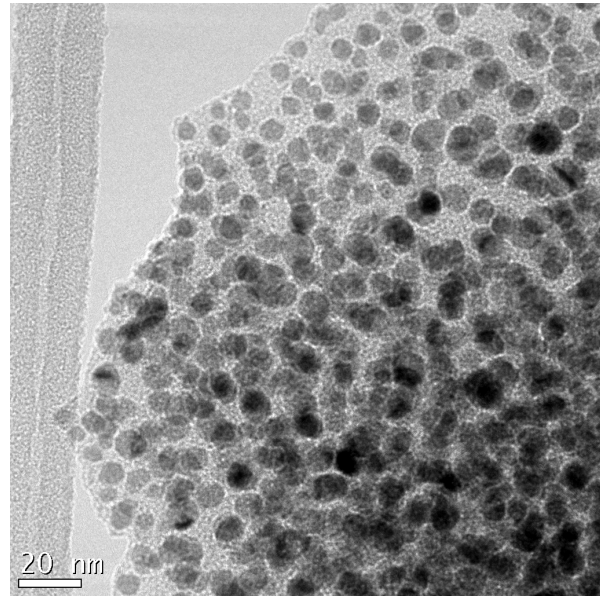
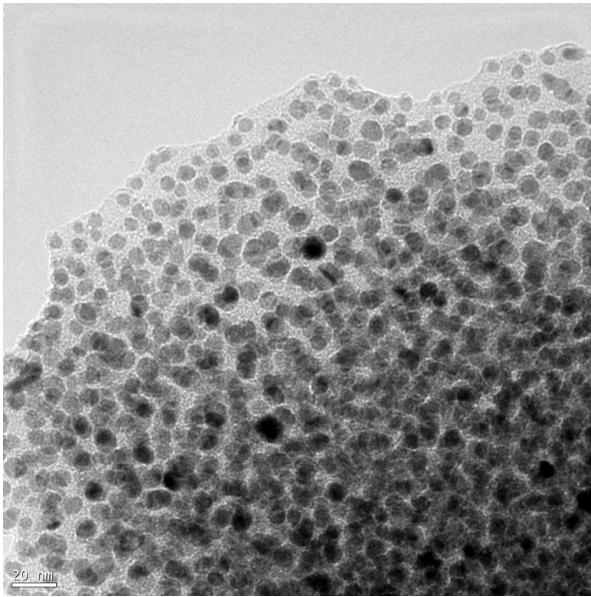


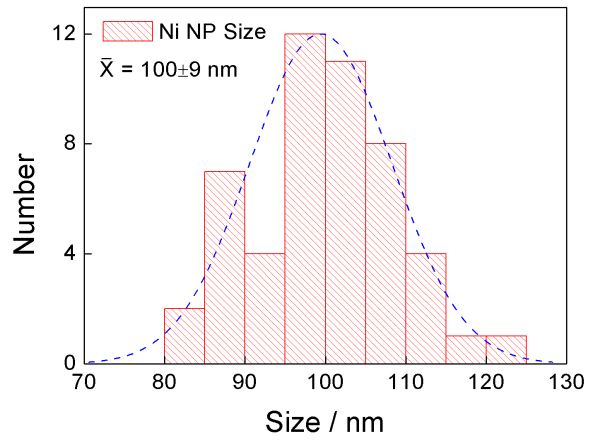
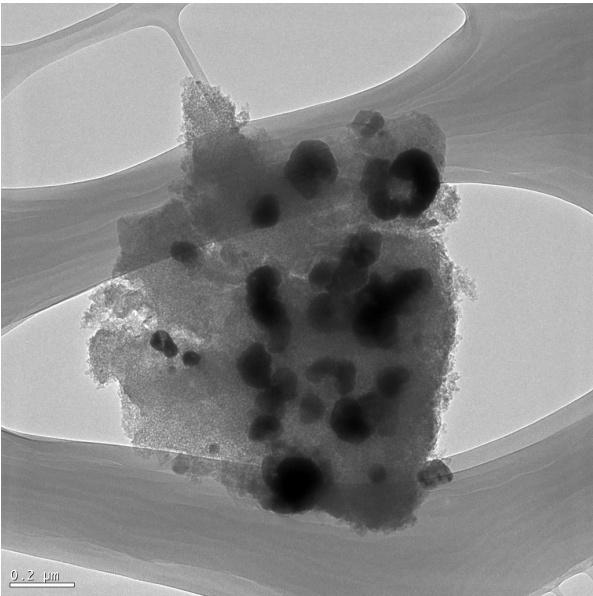
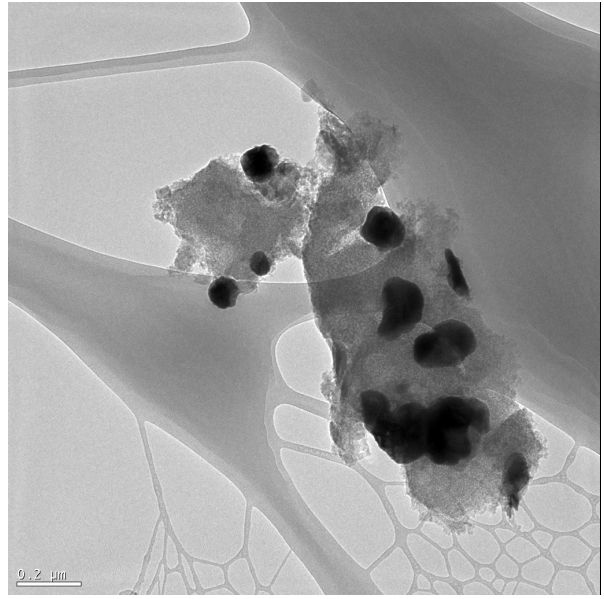
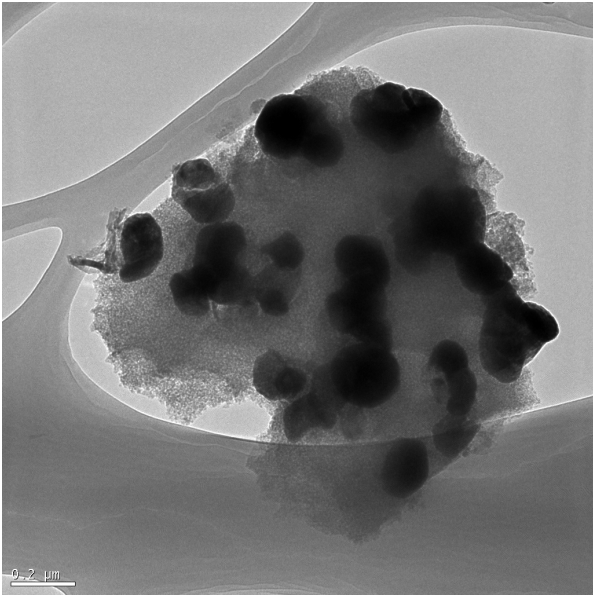
Ni/C<sub>1000</sub>:

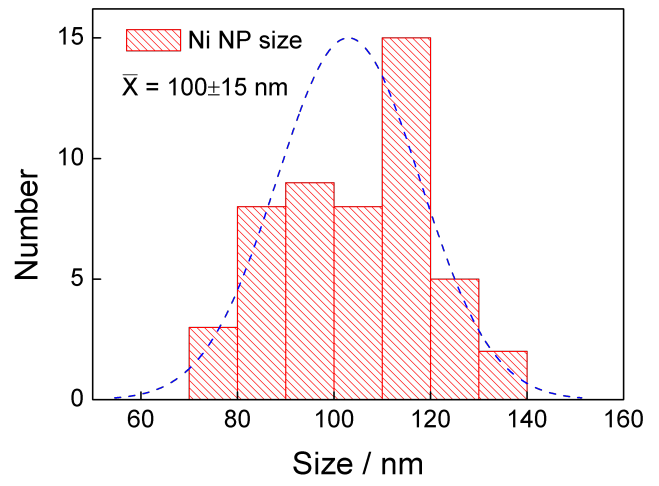
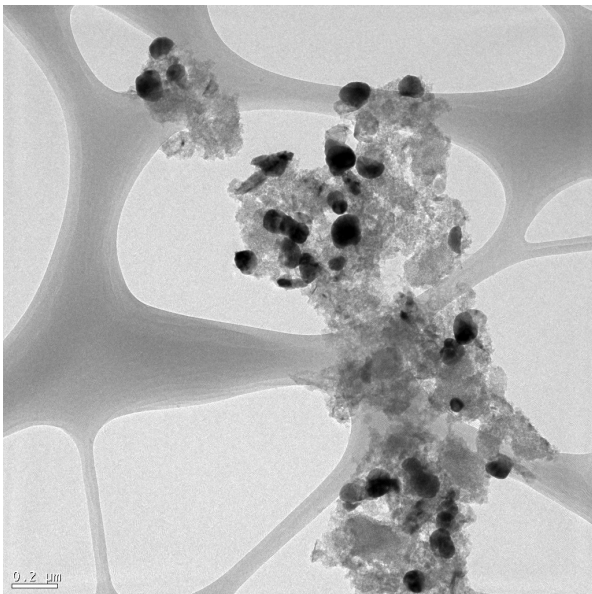
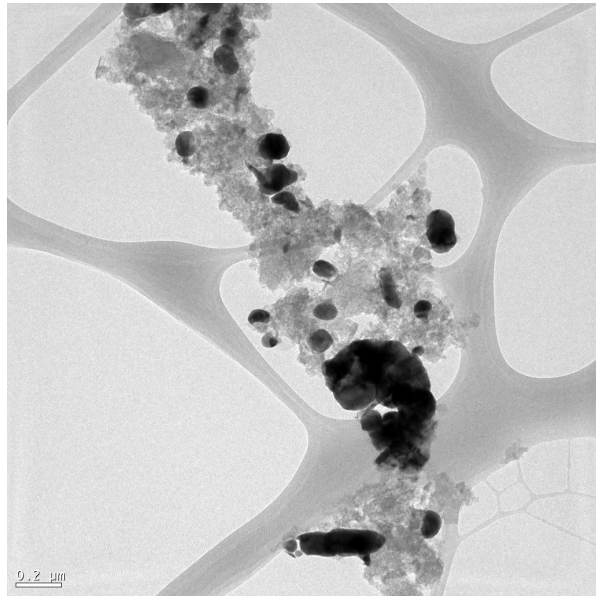
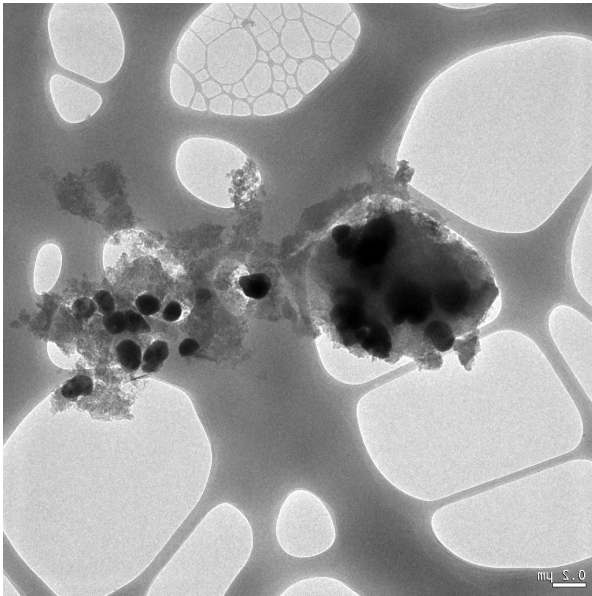


SI 11. TEM images of Ni/C<sub>450</sub>, Ni/C<sub>800</sub> and Ni/C<sub>1000</sub>. Size distribution of nanoparticles was estimated by optical analysis of these images by using ImageJ for at least 50 nanoparticles representative of each sample.

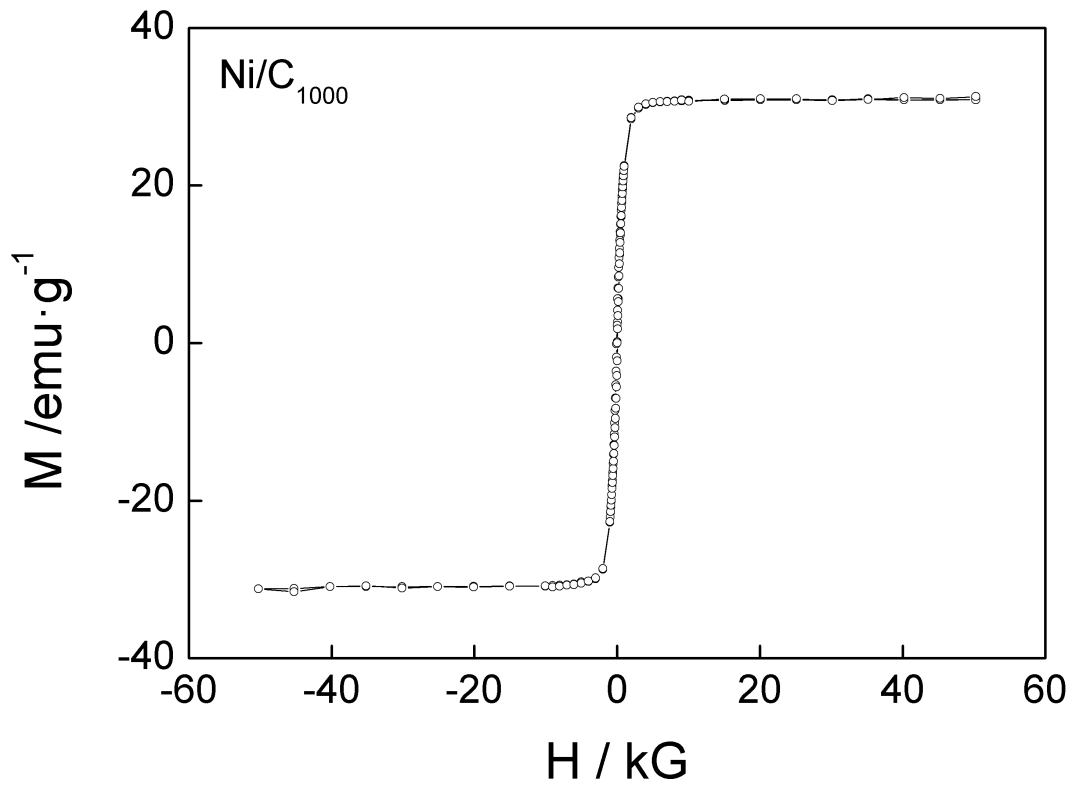
Ni/C<sub>450</sub>



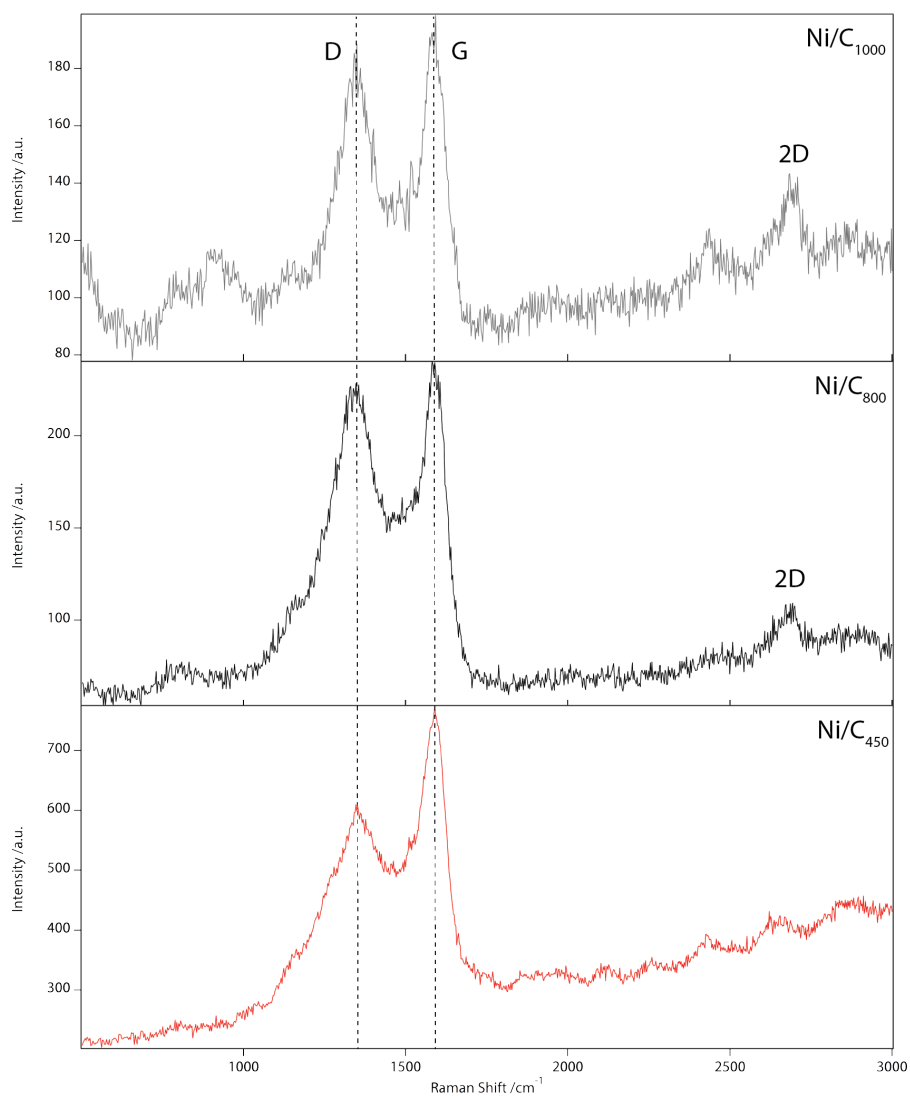




SI 12. Field dependence of the magnetization at 300 K of Ni/C<sub>1000</sub>.



SI 13. Raman spectra of Ni/C<sub>450</sub>, Ni/C<sub>800</sub> and Ni/C<sub>1000</sub> collected on bulk pellets at room temperature.

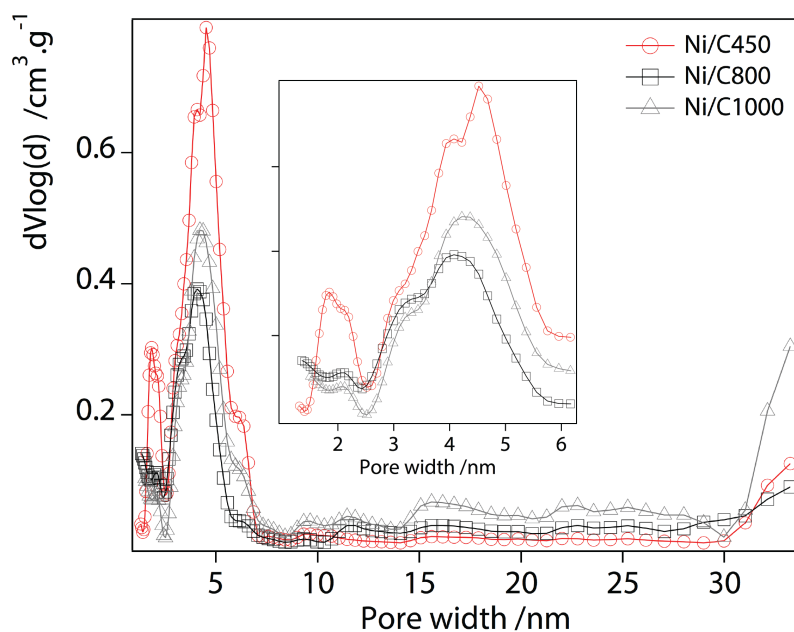
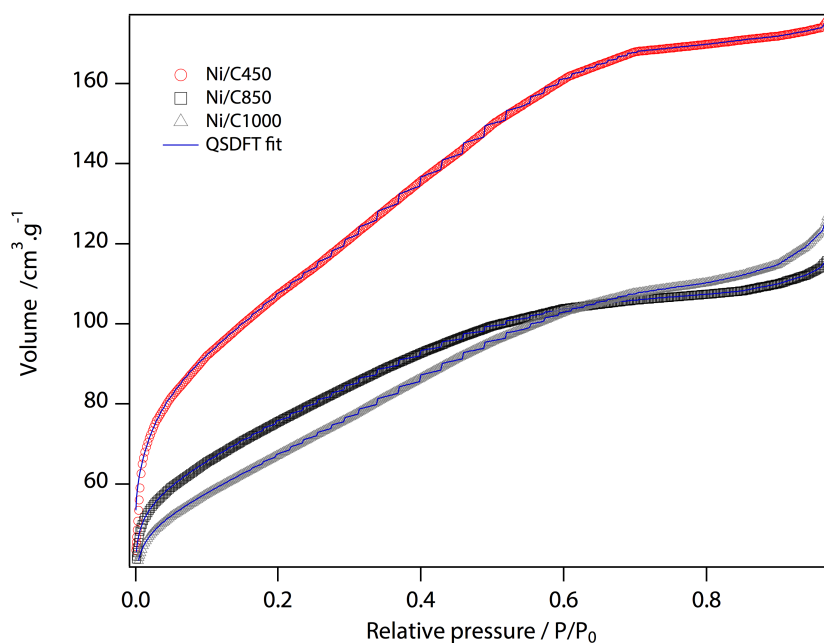


Sample	D band	G band	I <sub>G</sub> /I <sub>D</sub>	2D band
Ni/C <sub>450</sub>	1349	1592	1.27	N/A
Ni/C <sub>800</sub>	1347	1590	1.05	2686
Ni/C <sub>1000</sub>	1349	1588	1.05	2682

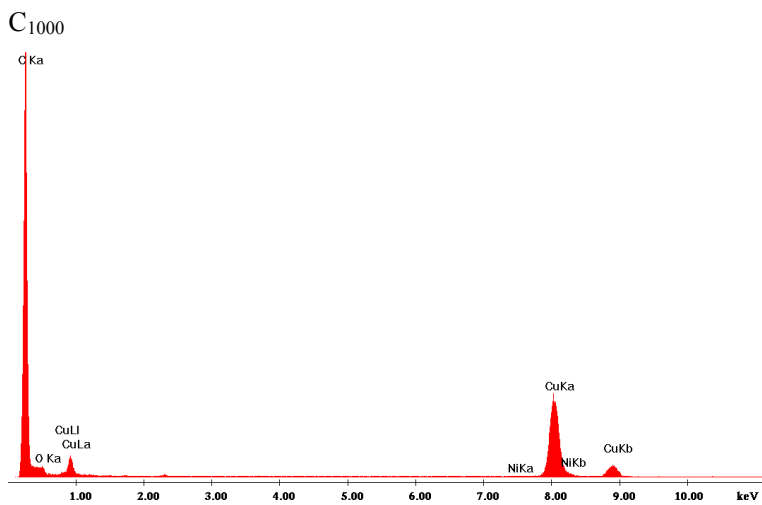
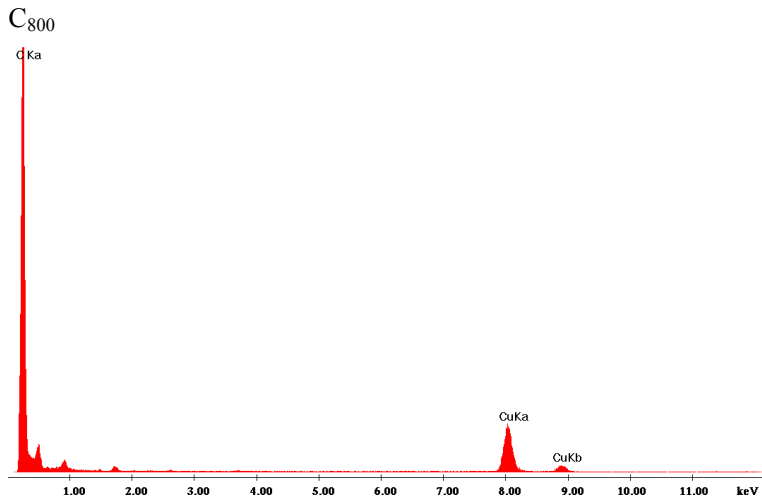
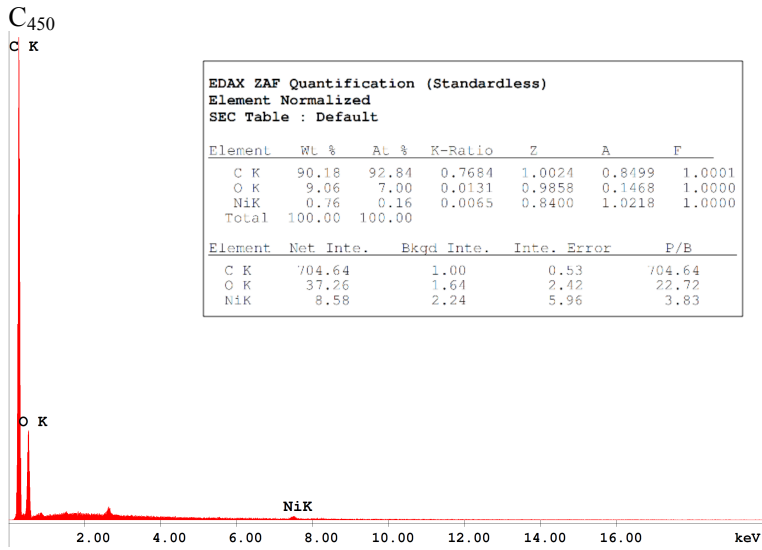
SI 14. Analysis of N<sub>2</sub> adsorption/desorption isotherms at 77K of Ni/C<sub>450</sub>, Ni/C<sub>800</sub> and Ni/C<sub>1000</sub>.

Sample	SA <sub>BET</sub> <sup>a</sup> (m <sup>2</sup> .g <sup>-1</sup> )	V <sub>t</sub> <sup>b</sup> (cm <sup>3</sup> .g <sup>-1</sup> )	V <sub>micro</sub> <sup>c</sup> (cm <sup>3</sup> .g <sup>-1</sup> )	V <sub>meso</sub> <sup>d</sup> (cm <sup>3</sup> .g <sup>-1</sup> )	PSD <sub>QSDFT</sub> (nm) <sup>e</sup>	
					micro	meso
C/Ni <sub>450</sub>	383	0.282	0.143	0.139	1.8	4.5
C/Ni <sub>800</sub>	268	0.188	0.099	0.089	2.0	4.2
C/Ni <sub>1000</sub>	239	0.226	0.084	0.142	2.0	4.0

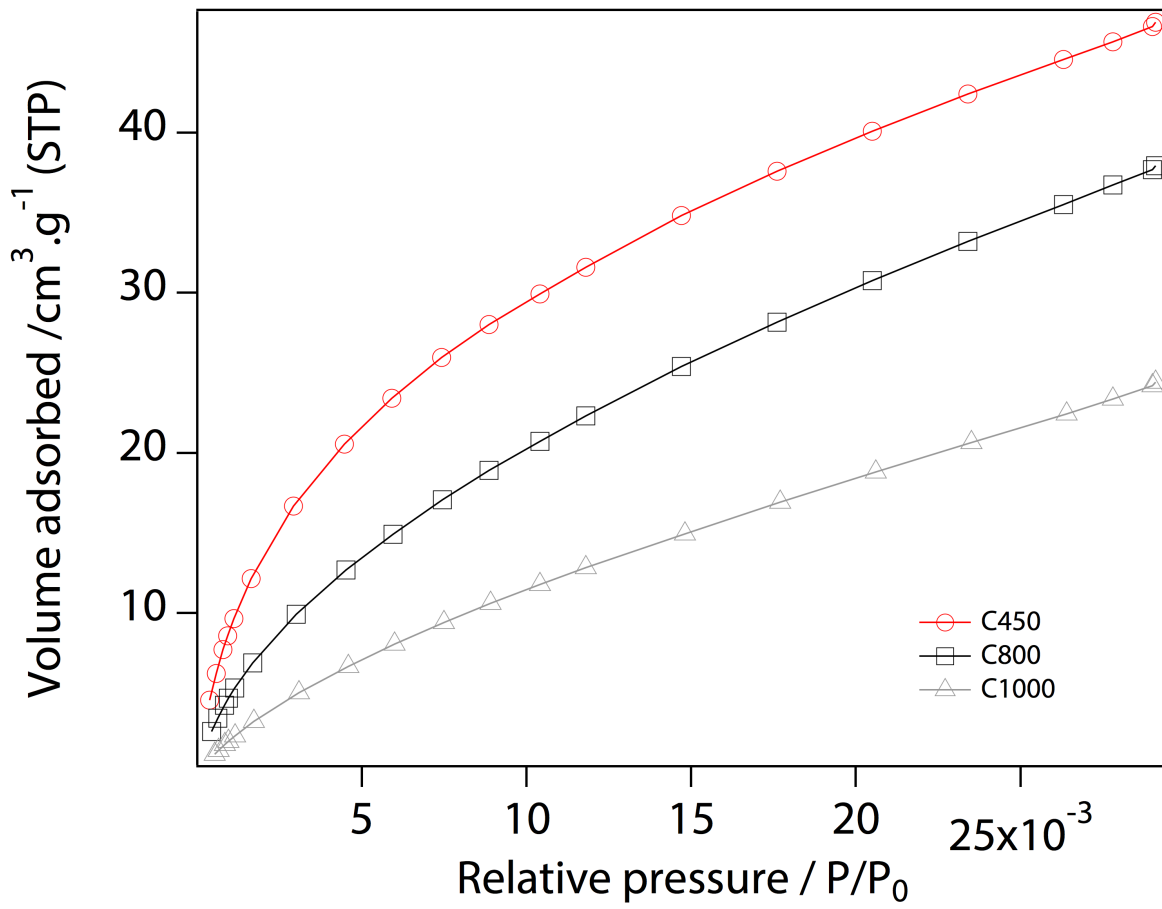
<sup>a</sup> Specific surface area (SA) was calculated by multi-point Brunauer-Emmett-Teller (BET) method. <sup>b</sup> Total pore volume at P/P<sub>0</sub>=0.96. <sup>c</sup> Micropore volume calculated with the Dubinin-Radushkevich (DR) equation. <sup>d</sup> Meso-pore volume (V<sub>meso</sub>) was calculated as the difference of total (V<sub>t</sub>) at P/P<sub>0</sub> = 0.96 and micropore volume (V<sub>micro</sub>). <sup>e</sup> Pore size distribution was analysed by using the solid density functional theory (QSDFT) for the adsorption branch assuming a cylindrical pore model. Fitting error was below 0.25% for all cases. See fit to experimental data and PSD of Ni/C composites below.



SI 15. Electron Probe Microanalysis of C<sub>450</sub>, C<sub>800</sub> and C<sub>1000</sub> to confirm complete metal leaching after acid treatment of the Ni/C composites. Cu signal in C<sub>800</sub> and C<sub>1000</sub> comes from the holder used in the SEM used for analysis.



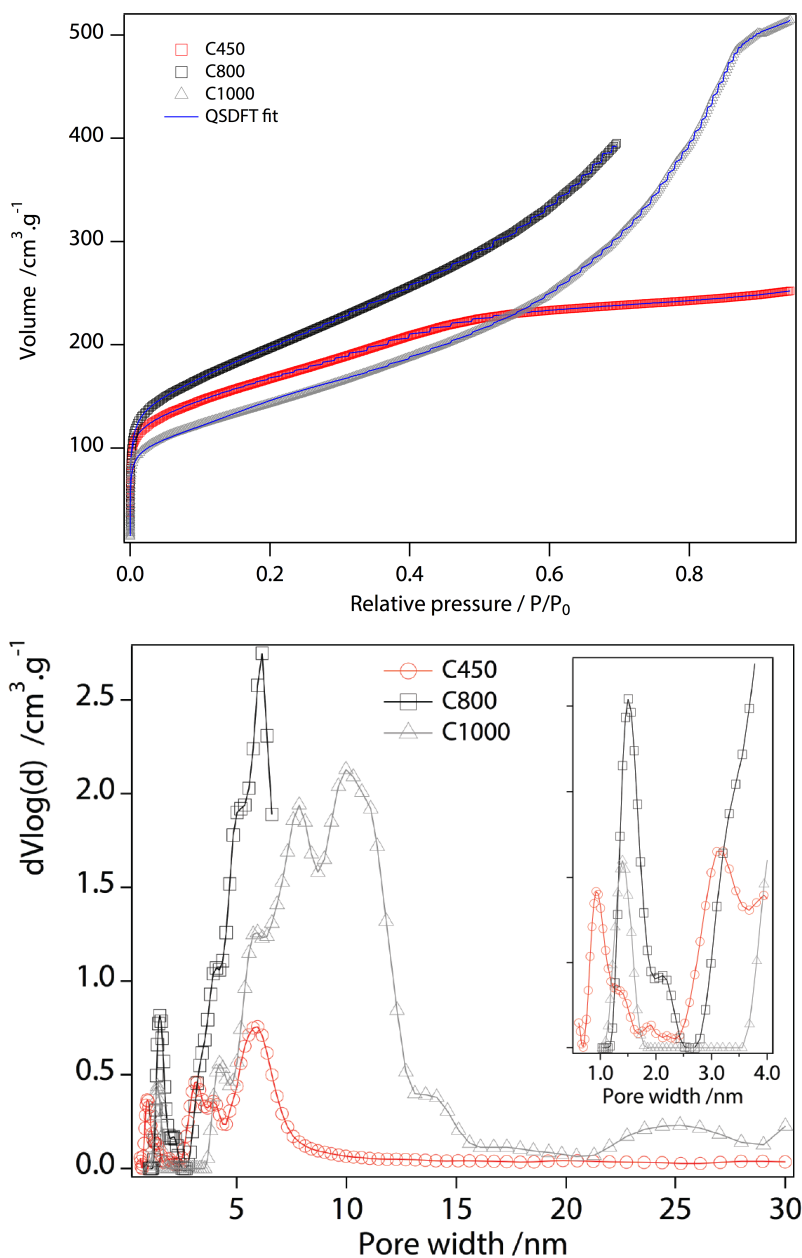
SI 16. CO<sub>2</sub> adsorption isotherms at 273K of C<sub>450</sub>, C<sub>800</sub> and C<sub>1000</sub>.



SI 17. Analysis of N<sub>2</sub> and CO<sub>2</sub> adsorption/desorption isotherms at 77 and 273K of C<sub>450</sub>, C<sub>800</sub> and C<sub>1000</sub>.

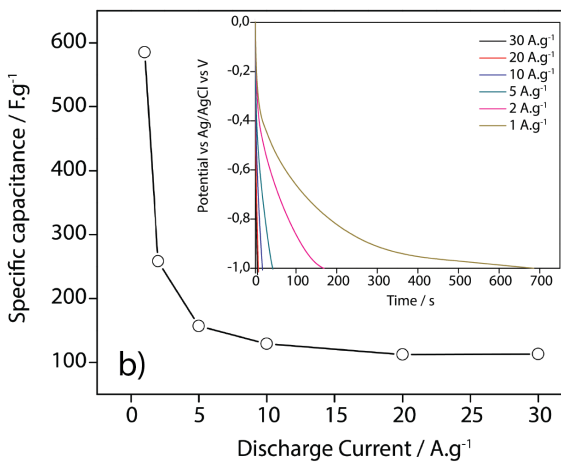
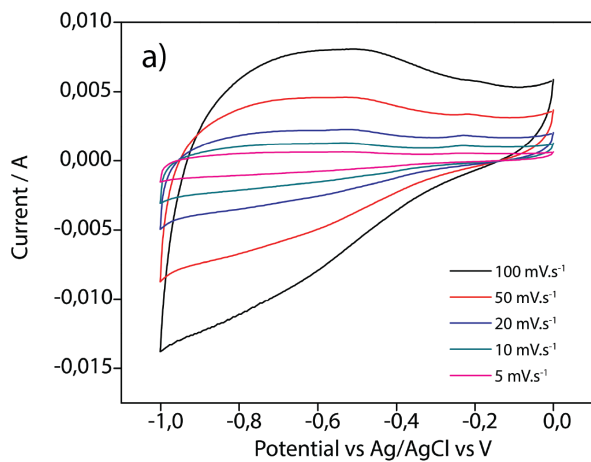
Sample	SA <sub>BET</sub> <sup>a</sup> (m <sup>2</sup> .g <sup>-1</sup> )	V <sub>t</sub> <sup>b</sup> (cm <sup>3</sup> .g <sup>-1</sup> )	V <sub>micro</sub> <sup>c</sup> N <sub>2</sub> (<2nm) (cm <sup>3</sup> .g <sup>-1</sup> )	V <sub>micro</sub> <sup>c</sup> CO <sub>2</sub> (<0.7nm) (cm <sup>3</sup> .g <sup>-1</sup> )	%micro <0.7nm	V <sub>meso</sub> <sup>d</sup> (cm <sup>3</sup> .g <sup>-1</sup> )	PSD <sub>QSDFT</sub> (nm) <sup>e</sup>	
							micro	meso
C <sub>450</sub>	587	0.394	0.207	0.146	70.5	0.187	0.9	3.0, 6.0
C <sub>800</sub>	706	0.840	0.260	0.105	40.4	0.580	1.5	>5.0
C <sub>1000</sub>	509	0.815	0.200	0.076	38.0	0.615	1.4	>5.0

<sup>a</sup> Specific surface area (SA) was calculated by multi-point Brunauer-Emmett-Teller (BET) method. <sup>b</sup> Total pore volume at P/P<sub>0</sub>=0.96. <sup>c</sup> Micropore volume calculated with the Dubinin-Radushkevich (DR) equation. N<sub>2</sub> isotherms at 77K were used for estimating total micropore volume whilst CO<sub>2</sub> at 273K accounts for micropores smaller than 0.7 nm not accessible to N<sub>2</sub>. <sup>d</sup> Mesopore volume (V<sub>meso</sub>) was calculated as the difference of total (V<sub>t</sub>) at P/P<sub>0</sub> = 0.96 and N<sub>2</sub> micropore volume (V<sub>micro</sub>). <sup>e</sup> Pore size distribution was analysed by using the solid density functional theory (QSDFT) for the adsorption branch assuming a cylindrical pore model. Fitting error was below 0.25% for all cases. See fit to experimental data and PSD of metal-free carbons below.

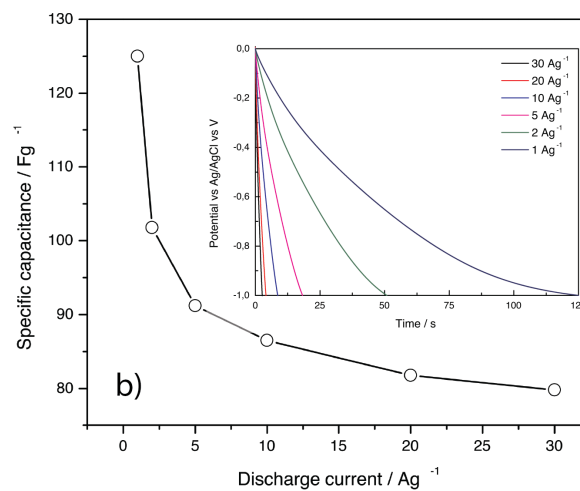
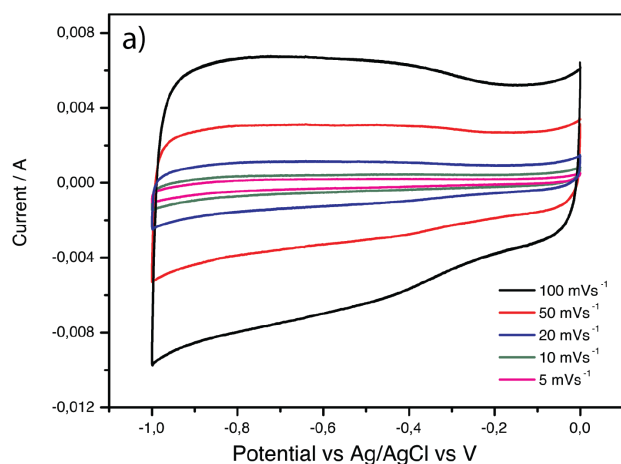


SI 18. Electrochemistry of  $C_{450}$  (top),  $C_{800}$  (middle) and  $C_{1000}$  (bottom). a) Three-electrode CVs at variable scan speed (5-1000  $\text{mV}\cdot\text{s}^{-1}$ ) in a 6 M KOH (aq) electrolyte. b) Evolution of the specific capacitance with discharge current (1-30  $\text{A}\cdot\text{g}^{-1}$ ) calculated from galvanostatic discharge curves (inset).

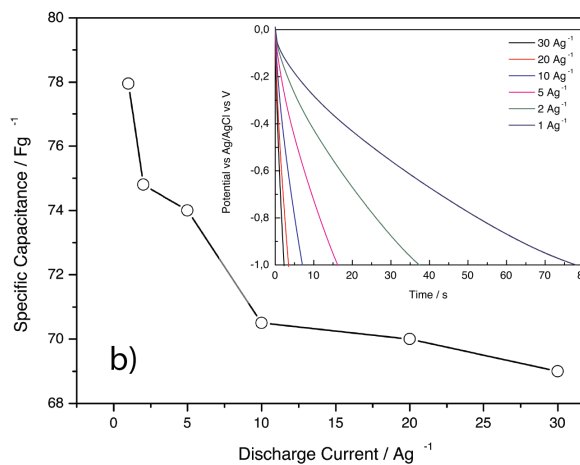
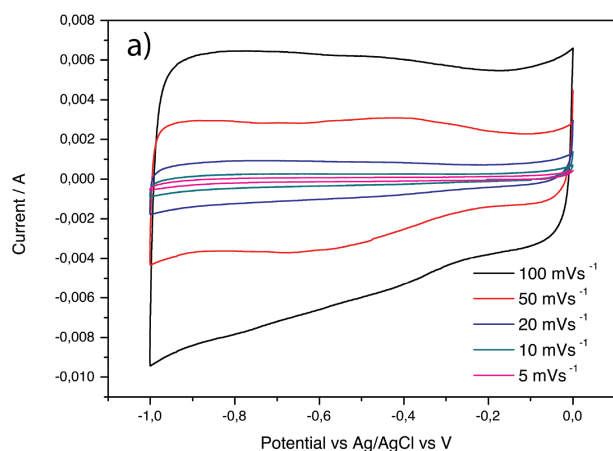
$C_{450}$



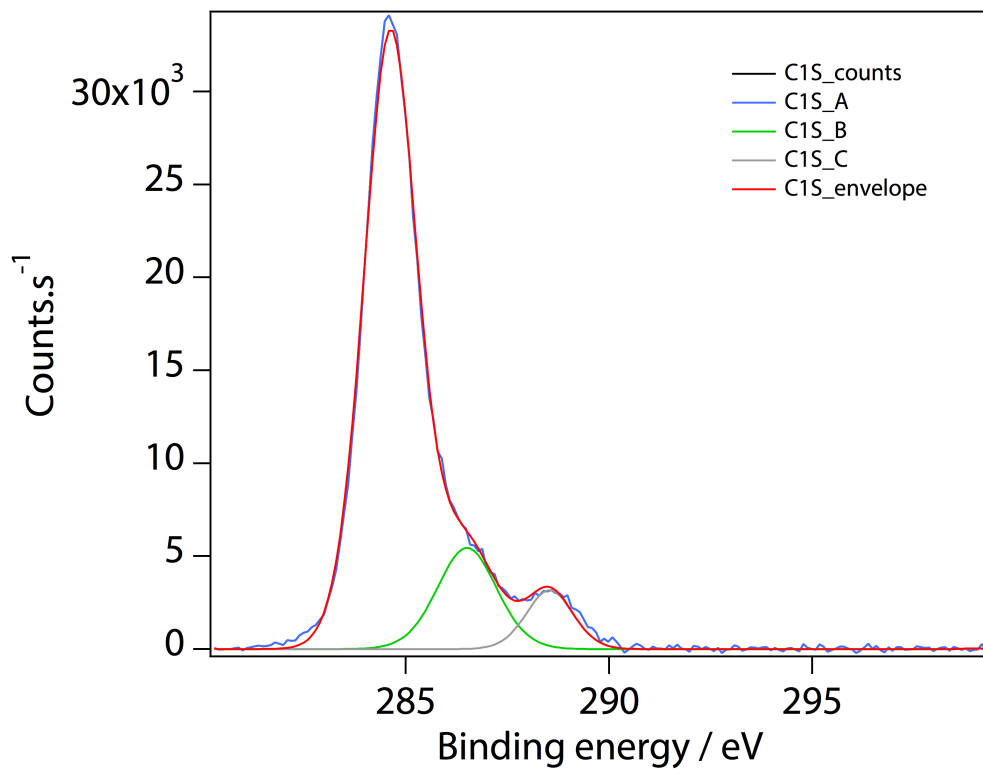
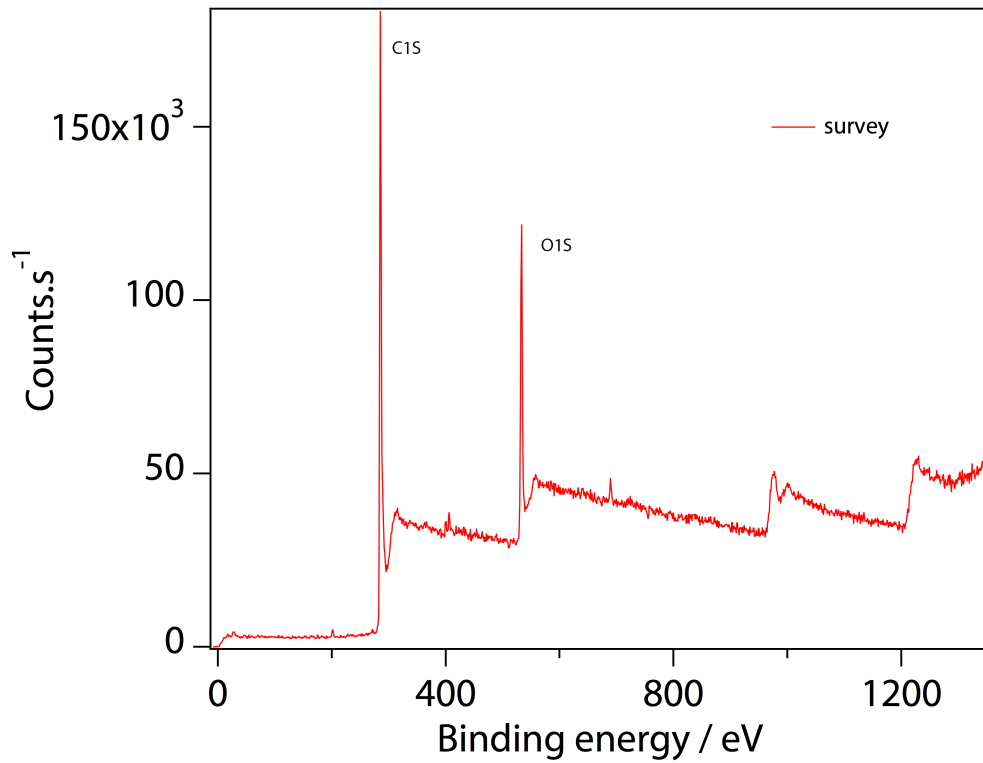
$C_{800}$

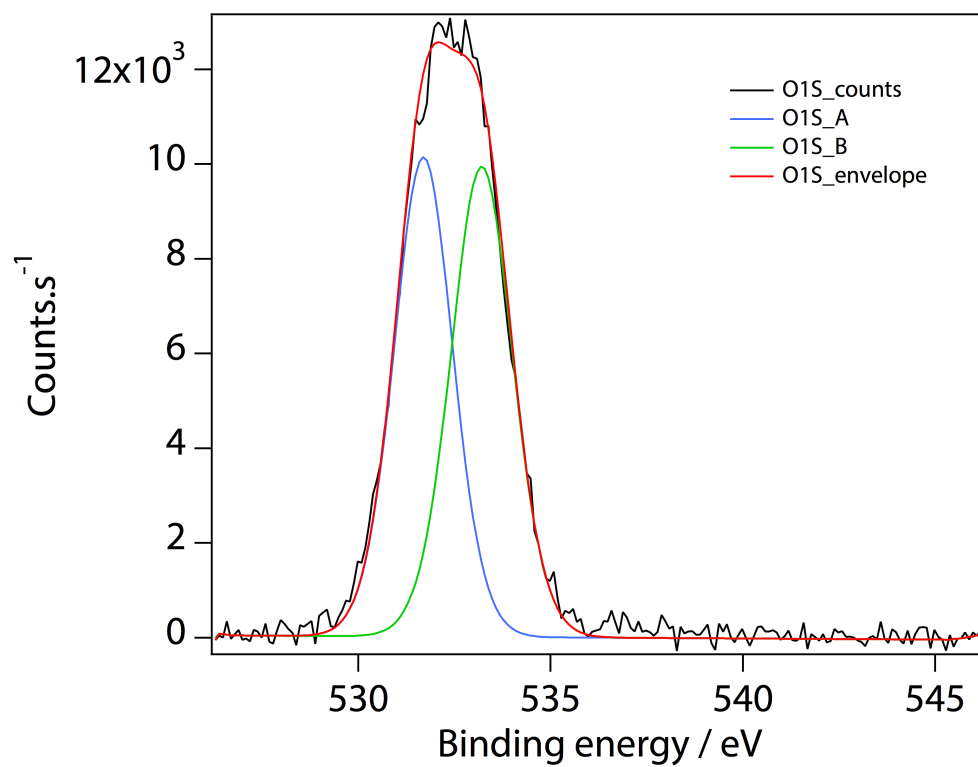


$C_{1000}$



SI 19. XPS spectra of C<sub>450</sub>. From top to bottom: survey, C1S and O1S spectra and table summarising XPS fitting model and C/O atomic ratio. Survey spectrum also confirms complete removal of Ni after acid treatment of Ni/C<sub>450</sub>.





	C1S			O1S	
Binding energies (eV)	284.6	286.50	288.54	531.69	533.21
Assignment	C-C	C-O	C=O	C=O	C-O
Rel. %	66.92	13.08	6.63	6.43	6.93
<sup>a</sup> Total %	86.6			13.4	

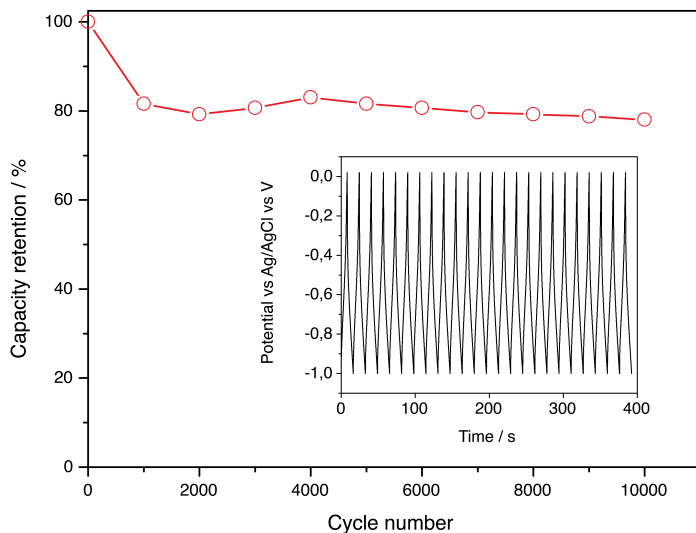
SI 20. Specific capacitances, textural properties and calcination temperatures of a representative set of MOF-derived carbons measured in a three-electrode system.

MOF template	Guest	T (°C)	S <sub>BET</sub> (m <sup>2</sup> .g <sup>-1</sup> )	V (cm <sup>3</sup> .g <sup>-1</sup> )	C (F.g <sup>-1</sup> )	Electrolyte	Reference
Ni-MOF-74	FA	450	482	0.34	585 at 1 A.g <sup>-1</sup>	KOH(aq) 6M	This work
ZIF-8	-	800	720	0.37	130 at 50 mV.s <sup>-1</sup>	H <sub>2</sub> SO <sub>4</sub> (aq) 0.5M	4
ZIF-8	FA	800	2169	1.50	188 at 5 mV.s <sup>-1</sup>	H <sub>2</sub> SO <sub>4</sub> (aq) 1M	5
MOF-5	Gly	950	2587	3.14	344 at 50 mA.g <sup>-1</sup>	KOH(aq) 6M	6
MOF-2	-	1000	1378	-	170 at 1 A.g <sup>-1</sup>	H <sub>2</sub> SO <sub>4</sub> (aq) 1M	7
HKUST	-	800	50	1.46	82.9 at 1 A.g <sup>-1</sup>	KOH(aq) 30%	8
Al-PCP	-	800	1103	1.04	173.6 at 1 A.g <sup>-1</sup>	KOH(aq) 30%	8
ZIF-67	-	800	943	0.84	238 at 20 mV.s <sup>-1</sup>	H <sub>2</sub> SO <sub>4</sub> (aq) 0.5M	9

T, temperature; SBET, Brunauer-Emmet-Teller surface area, V, pore volume; C, specific capacitance; FA, furfuryl alcohol; Gly, glycerol; en, ethylenediamine.

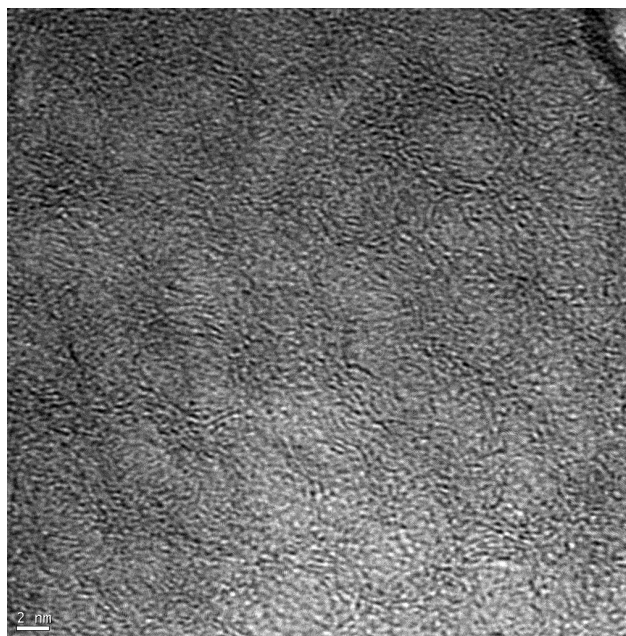
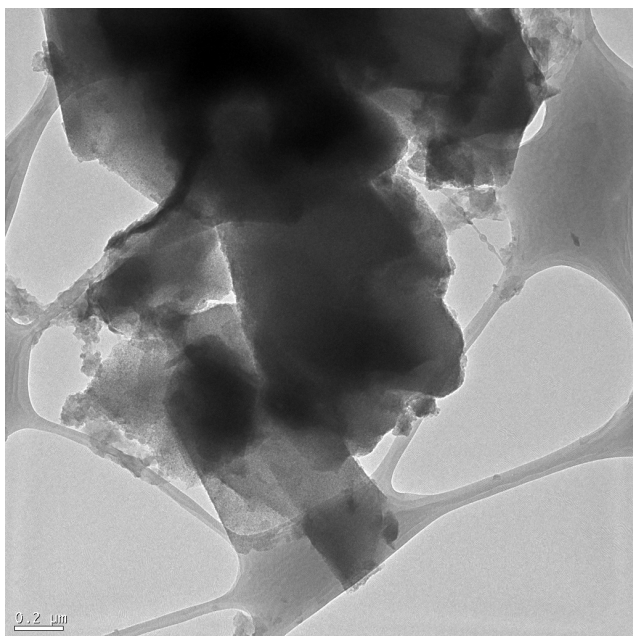
SI 21. Long-term stability cycling of  $C_{450}$  studied at  $10 \text{ A.g}^{-1}$  upon 10.000 charge-discharge cycles.

Long-term cyclability stands for close to 80% capacity retention. We believe this is due to mechanical detachment of the carbon particles from the electrode upon charge-discharge cycling. Electrode was prepared by drying and pressing a paste made by combining carbon with acetylene black and PVDF, deposited on a nickel foam electrode.

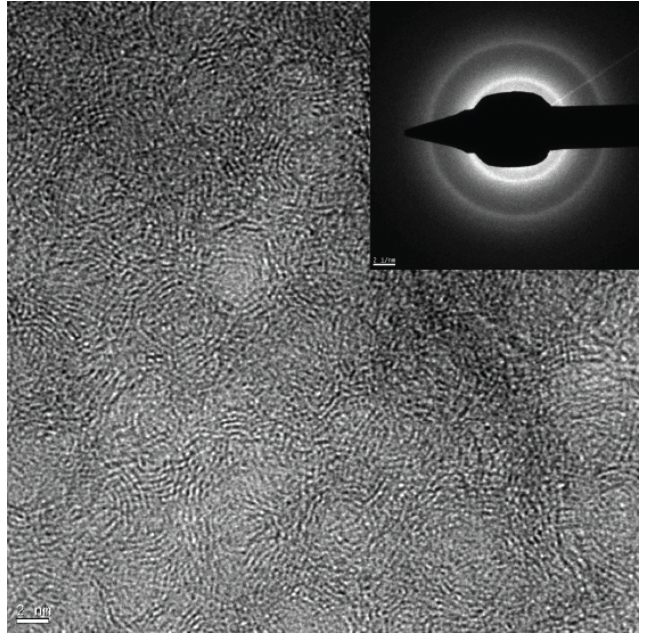
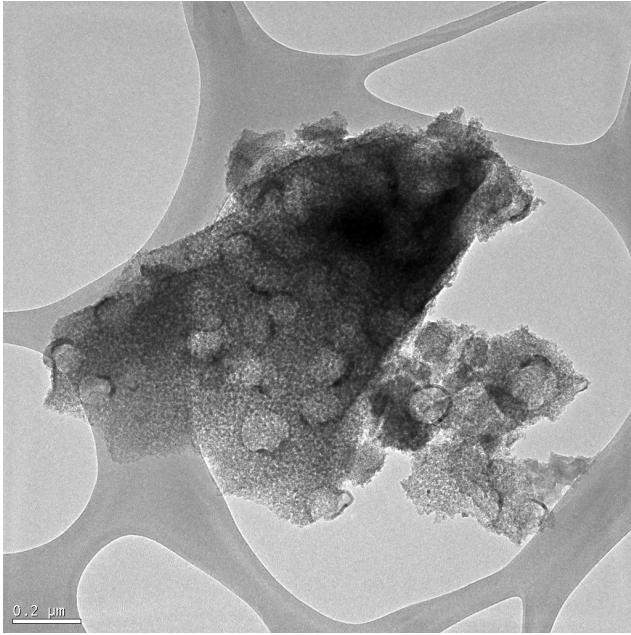


SI 22. High-Resolution Transmission Electron Microscopy study of carbons confirming the amorphous nature of  $C_{450}$  that becomes more graphitic at higher calcination temperatures.

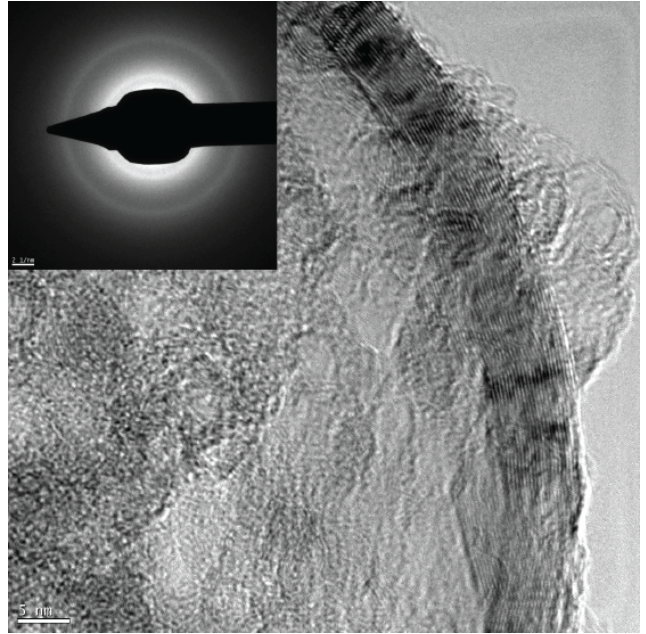
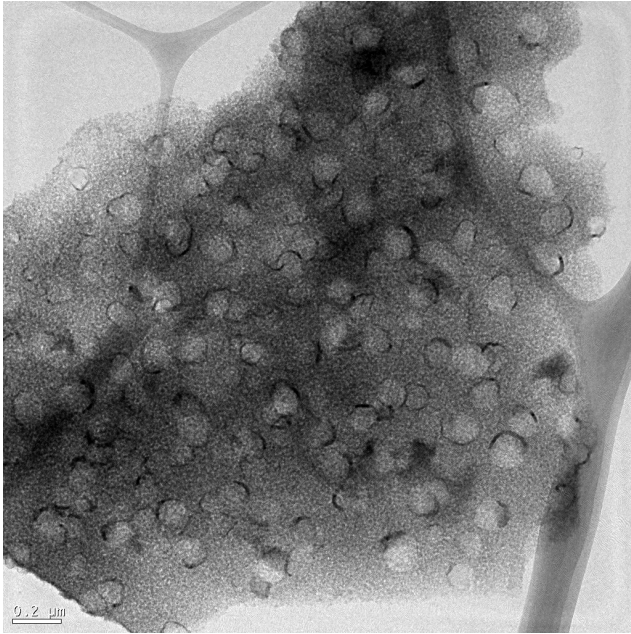
$C_{450}$



$C_{800}$



C<sub>1000</sub>



SI30

SI 23. References.

- 1 S. R. Caskey, A. G. Wong-Foy and A. J. Matzger, *J. Am. Chem. Soc.*, 2008, **130**, 10870–10871.
- 2 P. D. C. Dietzel, B. Panella, M. Hirscher, R. Blom and H. Fjellvåg, *Chem. Commun.*, 2006, 959-961.
- 3 D.-A. Yang, H.-Y. Cho, J. Kim, S.-T. Yang and W.-S. Ahn, *Energy & Environ. Sci.*, 2012, **5**, 6465–6473.
- 4 W. Chaikittisilp, M. Hu, H. Wang, H.-S. Huang, T. Fujita, K. C. W. Wu, L.-C. Chen, Y. Yamauchi and K. Ariga, *Chem. Commun.*, 2012, **48**, 7259–7261.
- 5 H.-L. Jiang, B. Liu, Y.-Q. Lan, K. Kuratani, T. Akita, H. Shioyama, F. Zong and Q. Xu, *J. Am. Chem. Soc.*, 2011, **133**, 11854–11857.
- 6 D. Yuan, J. Chen, S. Tan, N. Xia and Y. Liu, *Electrochemistry Communications*, 2009, **11**, 1191–1194.
- 7 H. B. Aiyappa, P. Pachfule and R. Banerjee, *Cryst. Growth Des.*, 2013, **13**, 4195–4199.
- 8 X. Yan, X. Li, Z. Yan and S. Komarneni, *App. Surf. Sci.*, 2014, **308**, 306–310.
- 9 N. L. Torad, R. R. Salunkhe, Y. Li, H. Hamoudi, M. Imura, Y. Sakka, C. C. Hu and Y. Yamauchi, *Chem-Eur J.*, 2014, **20**, 7895–7900.